

# Beyond maps: Patterns of formation processes at the Middle Pleistocene open-air site of Marathousa 1, Megalopolis Basin, Greece

D. Giusti<sup>a,\*</sup>, V. Tourloukis<sup>a</sup>, G. E. Konidaris<sup>a</sup>, N. Thompson<sup>a</sup>, P. Karkanas<sup>b</sup>,  
E. Panagopoulou<sup>c</sup>, K. Harvati<sup>a</sup>

<sup>a</sup>*Paläoanthropologie, Senckenberg Centre for Human Evolution and Palaeoenvironment, Eberhard Karls Universität Tübingen, Rümelinstr. 23, 72070 Tübingen, Germany*

<sup>b</sup>*Malcolm H. Wiener Laboratory for Archaeological Science, American School of Classical Studies at Athens, Greece*

<sup>c</sup>*Ephoreia of Palaeoanthropology-Speleology of Greece, Athens, Greece*

---

## Abstract

Recent excavations at the Middle Pleistocene open-air site of Marathousa 1 have unearthed in one of the two investigated areas (Area A) a partial skeleton of a single individual of *Palaeoloxodon antiquus* and other faunal remains in spatial and stratigraphic association with lithic artefacts. In Area B, a much higher number of lithic artefacts was collected, spatially and stratigraphically associated also with faunal remains. The two areas are stratigraphically correlated, the main fossiliferous layers representing an *en masse* depositional process in a lake margin context. Evidence of butchering (cut-marks) has been identified on bones of the elephant skeleton, as well on elephant and other mammal bones from Area B. However, due to the secondary deposition of the main find-bearing units, it is of primary importance to evaluate the degree and reliability of the spatial association of the lithic artefacts with the faunal remains. Indeed, spatial association does not necessarily imply causation, since natural syn- and post-depositional processes may equally produce spatial association. Assessing the degree and extent of post-depositional reworking processes is crucial to fully comprehend the archaeological record, and therefore to reliably interpret past human behaviours. The present study uses a comprehensive set of spatial statistics in order to disentangle the depositional processes behind the distribution of the archaeological and palaeontological record at Marathousa 1. Preliminary results of our analyses suggest that a high-energy erosional process, attributed to a hyperconcentrated flow deposited at the margin of a swamp, reworked an autochthonous, exposed or slightly buried, scatter of lithic artefacts and faunal remains. Minor reworking and substantial spatial association of the lithic and faunal assemblages support the current interpretation of Marathousa 1 as a butchering site.

**Keywords:** Spatial analysis, Site formation processes, Vertical distribution, Fabric

---

\*Corresponding author

Email address: domenico.giusti@uni-tuebingen.de (D. Giusti)

## 1. Introduction

2 Archaeological site formation processes, intensively studied since the early 1970s  
3 (Isaac, 1967; Schiffer, 1972, 1983, 1987; Shackley, 1978; Wood and Johnson, 1978;  
4 Binford, 1981; Schick, 1984, 1986, 1987; Petraglia and Nash, 1987; Petraglia and  
5 Potts, 1994, among others), “still insufficiently taken in consideration” (Texier, 2000,  
6 p.379) at the beginning of the 21st century, are nowadays fully acknowledged in the ar-  
7 chaeological practice (Villa, 2004; Bailey, 2007; Brantingham et al., 2007; Malinsky-  
8 Buller et al., 2011; Vaquero et al., 2012; Bargalló et al., 2016, among others). Drawing  
9 inferences about past human behaviours from scatters of archaeological remains must  
10 account for syn- and post-depositional contextual processes.

11 Several methods are currently applied in order to qualify and quantify the type and  
12 degree of reworking of archaeological assemblages. Within the framework of a geoar-  
13 chaeological and taphonomic approach, spatial statistics offer meaningful contributions  
14 in unravelling site formation and modification processes from spatial patterns. How-  
15 ever, while the spatio-temporal dimension is an ineluctable inherent property of any  
16 biotic and abiotic process, spatial statistics are still insufficiently applied.

17 Distribution maps are cornerstones of the archaeological documentation process  
18 and are primary analytic tools. However, their visual interpretation is prone to subjec-  
19 tivity and is not reproducible (Bevan et al., 2013). Since the early 1970's (see Hodder  
20 and Orton (1976); Orton (1982) and references therein), the traditional, intuitive, ‘eye-  
21 balling’ method of spotting spatial patterns has been abandoned in favour of more ob-  
22 jective approaches, extensively borrowed from other fields. Nevertheless, quantitative  
23 methods, while still percolating in the archaeological sciences from neighbouring dis-  
24 ciplines, are not extensively used. Moreover, only a relatively small number of studies  
25 have explicitly applied spatial point pattern analysis or geostatistics to the study of site  
26 formation and modification processes (Lenoble et al., 2008; Domínguez-Rodrigo et al.,  
27 2014b,a, 2017; Carrer, 2015; Giusti and Arzarello, 2016; Organista et al., 2017, but see  
28 Hivernel and Hodder (1984) for an earlier work on the subject).

29 The goal of a taphonomic approach to spatial analysis is to move beyond distri-  
30 bution maps by applying a comprehensive set of multiscale and multivariate spatial  
31 statistics in order to reliably construct inferences from spatial patterns. An exhaustive  
32 spatial analytic approach to archaeological inference, combined with a taphonomic  
33 perspective, is essential for evaluating the depositional processes and integrity of the  
34 archaeological assemblage, and consequently for a reliable interpretation of past hu-  
35 man behaviours.

36 The present study uses a comprehensive set of spatial statistics in order to disentan-  
37 gle the depositional processes behind the spatial distribution of the archaeological and  
38 palaeontological record recovered during excavation at the Middle Pleistocene open-air  
39 site of Marathousa 1, Megalopolis, Greece (Panagopoulou et al., 2015; Harvati et al.,  
40 2016).

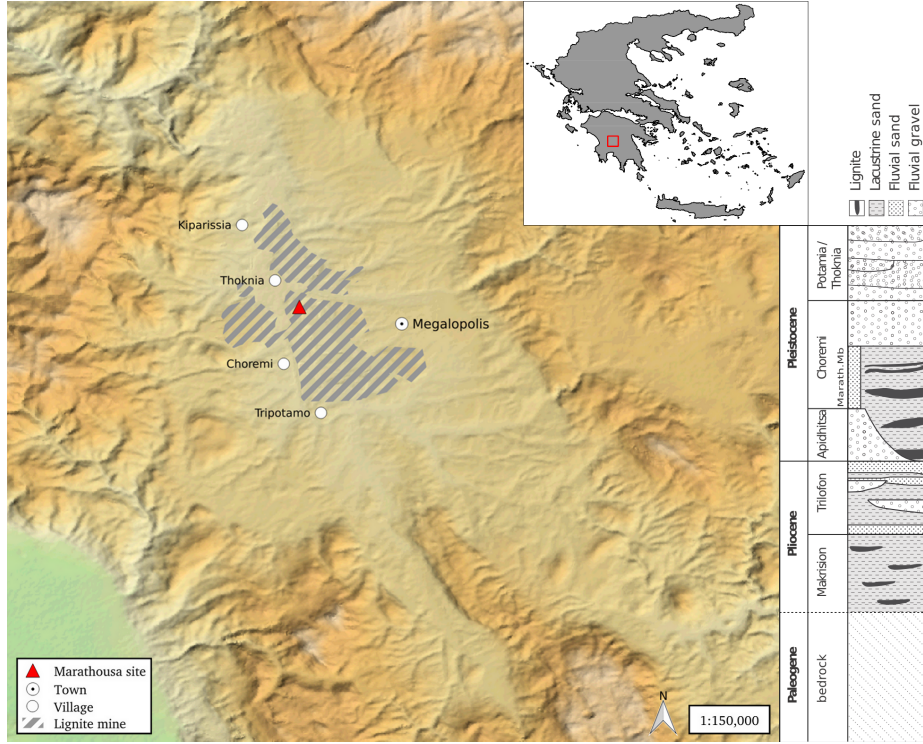


Figure 1: Geographical location of the Marathousa 1 site in the Megalopolis basin and stratigraphic column of the basin, modified after [van Vugt et al. \(2000\)](#).

### 41      1.1. Marathousa 1

42      The site (Fig. 1), discovered in 2013 at the edge of an active lignite quarry, is  
 43      located between two lignite seams in the Pleistocene deposits of the Megalopolis basin,  
 44      Marathousa Member of the Choremi Formation ([van Vugt et al., 2000](#)). The regular  
 45      alternation of lacustrine clay, silt and sand beds with lignite seams has been interpreted  
 46      having cyclic glacial (or stadial) and interglacial (or interstadial) origin ([Nickel et al.,  
 47      1996](#)). The half-graben configuration of the basin, with major subsidence along the  
 48      NW-SE trending normal faults along the eastern margin, resulted in the gentle dip of  
 49      the lake bottom at the opposite, western, margin of the lake, enabling the formation of  
 50      swamps and the accumulation of organic material for prolonged periods of time ([van  
 51      Vugt et al., 2000](#)).

52      Two excavation areas have been investigated since 2013 (Fig. 2): Area A, where  
 53      several skeletal elements of a single individual of *Palaeoloxodon antiquus* have been  
 54      unearthed, together with a number of lithic artefacts and other faunal remains; and  
 55      Area B, located 60 m to the South along the exposed section, where the lithic assem-  
 56      blage is richer and occurs in association with a faunal assemblage composed of isolated  
 57      elephant bones, cervids and carnivores among others. Bones from Area B are charac-  
 58      terized by a high degree of fragmentation (bone fragments make up 93.4% of the as-

59 semblage), with their maximal diameter mostly measuring less than 80mm ([Konidaris](#)  
60 [et al., this issue](#); [Tourloukis et al., this issue](#)). Evidence of butchering (cut-marks) have  
61 been identified on two of the elephant bones from Area A, as well on elephant and  
62 other mammal bones from Area B ([Konidaris et al., this issue](#)).

63 The sedimentary sequence of the site (Fig. 3) includes lacustrine and fluvio-lacustrine  
64 clastic deposits sandwiched between two lignite seams (UA7-UB10 and UA1-UB1)  
65 ([Karkanas et al., this issue](#)). A major hiatus (contacts between UA3 and UA4, and  
66 between UB5 and UB6), attributed to exposure and erosion of a lake shore mudflat,  
67 divides the sequence in two parts. The lower part is characterised by relatively high  
68 rate sub-aqueous sedimentation of bedded sands and silts, containing low organic and  
69 carbonate content. The upper one is characterised by a series of erosional bounded  
70 depositional units, attributed to sub-aerial originated organic- and carbonate-rich mud  
71 flows and hyperconcentrated flows deposited at the margin of a swamp ([Karkanas et al.,](#)  
72 [this issue](#)).

73 The erosional contacts UA3c/4 and UB4c/5a separate the two main find-bearing  
74 units in both areas (Fig. 3). In Area A, the elephant remains lie at the contact of UA3c/4  
75 and are covered by UA3c (Fig. 4a); while in Area B, most of the remains were collected  
76 from unit UB4c (Figs. 2 and 4b). Units UA3c and UB4c (organic- and intraclast-rich  
77 silty sands) resemble dilute mud flows, showing a chaotic structure of rip-up clasts  
78 from the underlying unit, small-to-large wood fragments and rare rock clasts. In Area  
79 B, a relatively low number of remains was also found in massive organic-rich silty  
80 sands (UB5a, Fig. 2), which locally overlay channelised sands (UB5b/c), probably not  
81 preserved in Area A ([Karkanas et al., this issue](#)).

82 The flow event described above (units UA3c and UB4c), and specifically the ero-  
83 sional contacts between the fossiliferous horizons in the two areas (UA3c/4 and UB4c/5a),  
84 provide the essential background for the analysis and interpretation of the spatial dis-  
85 tributions at Marathousa 1.

86 The secondary depositional nature of the main find horizons raises the question  
87 of how reliable is the spatial association between the lithic artefacts and the partial  
88 skeleton of a single *Palaeoloxodon antiquus* individual and other faunal remains. Since  
89 spatial association does not necessarily imply causation, and consequently synchrony,  
90 the answer has important consequences for the interpretation of the site in the broader  
91 context of the Middle Pleistocene human-proboscidean interactions. We aim to tackle  
92 this question and disentangle the formation processes acting at Marathousa 1 on the  
93 basis of spatial patterns through a three-prong spatial analytic approach:

- 94 1. by analysing, in a frame of references, the orientation patterns of remains from  
95 relevant stratigraphic units;
- 96 2. by quantifying and comparing their relative vertical distributions;
- 97 3. by identifying spatial trends in either the assemblage intensities and the associa-  
98 tions between classes of remains.

99 Two contrasting models of deposition are tested: the autochthonous hypothesis  
100 (*sensu* [Fernández-López, 1991](#); [Domínguez-Rodrigo et al., 2012](#)) states that the flow  
101 event, represented by units UA3c and UB4c, eroded and scoured the exposed surface  
102 (where the elephant was lying), thereby entraining clastic material (including arte-  
103 facts) and re-depositing (*sensu* [Fernández-López, 1991](#)) this material at a close dis-

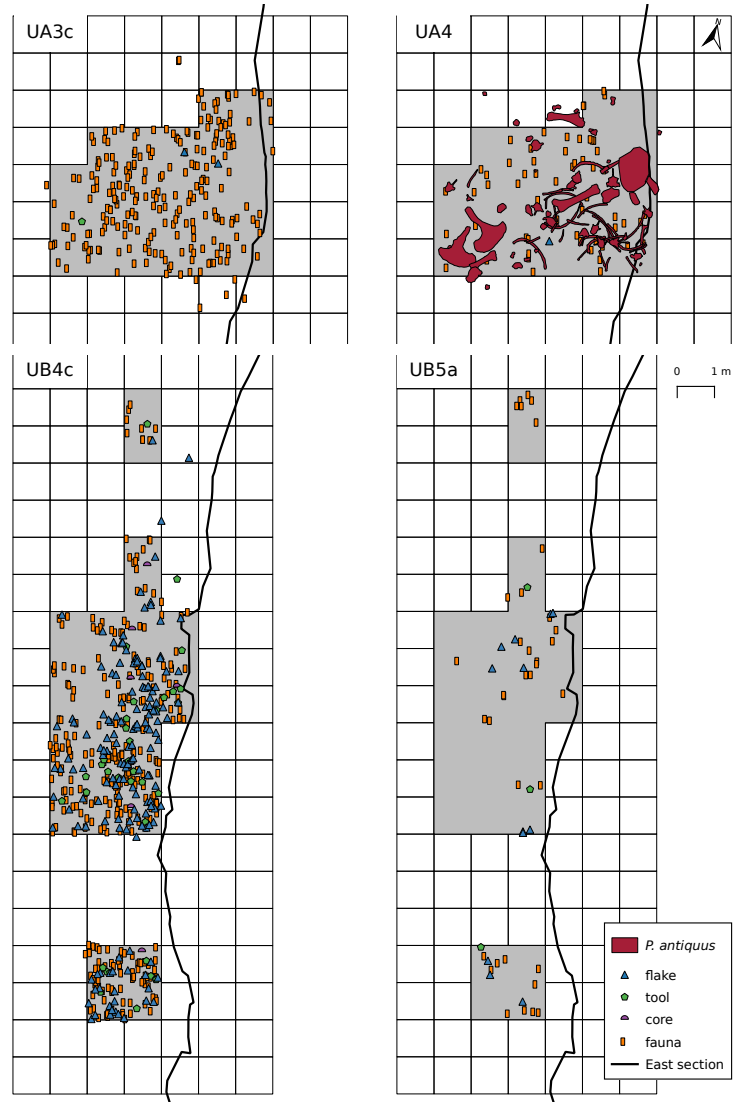


Figure 2: Distribution maps of the plotted remains from areas A (units UA3c and UA4) and B (units UB4c and UB5a), collected until 2015. Due to their high number, lithic debris/chips are not plotted. The plotted remains of the *P. antiquus* skeleton were collected until 2016. Grey zones mark the 2013-2015 excavation areas. Area B is located 60 m to the South, along the exposed East section of the lignite quarry.

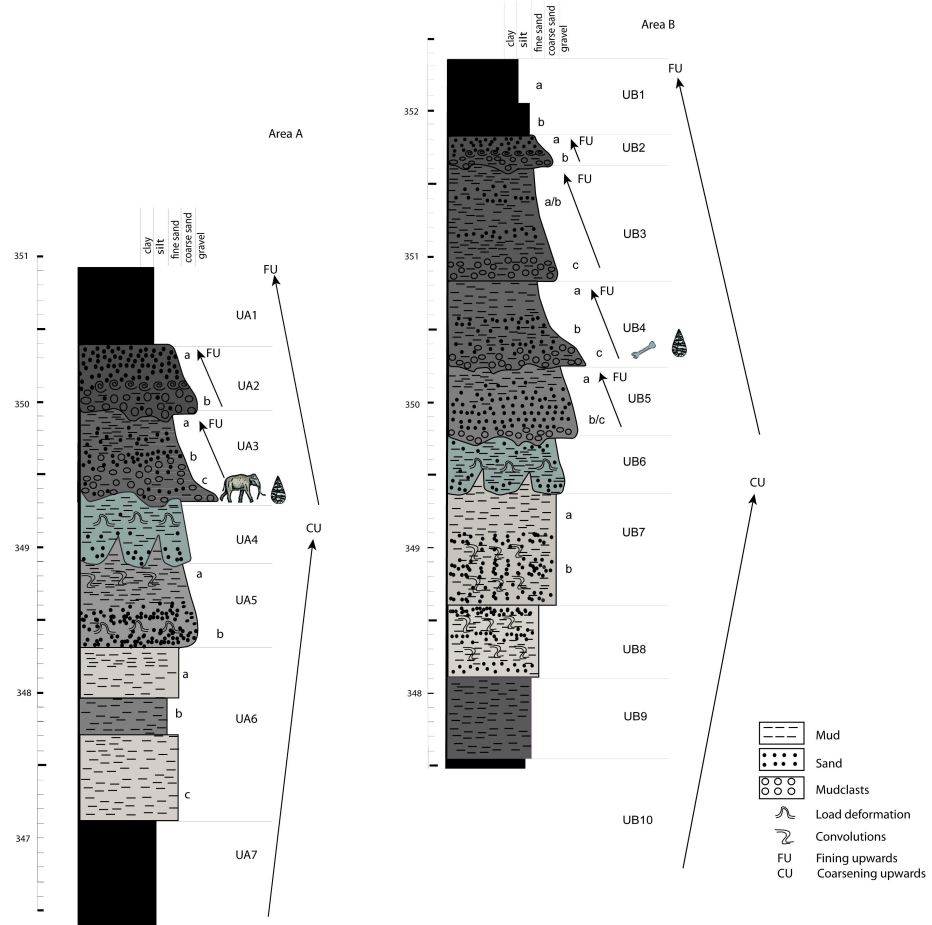


Figure 3: Stratigraphic setting of the Marathousa 1 site, modified after Karkanas et al. ([this issue](#)). Absolute elevations in m a.s.l.

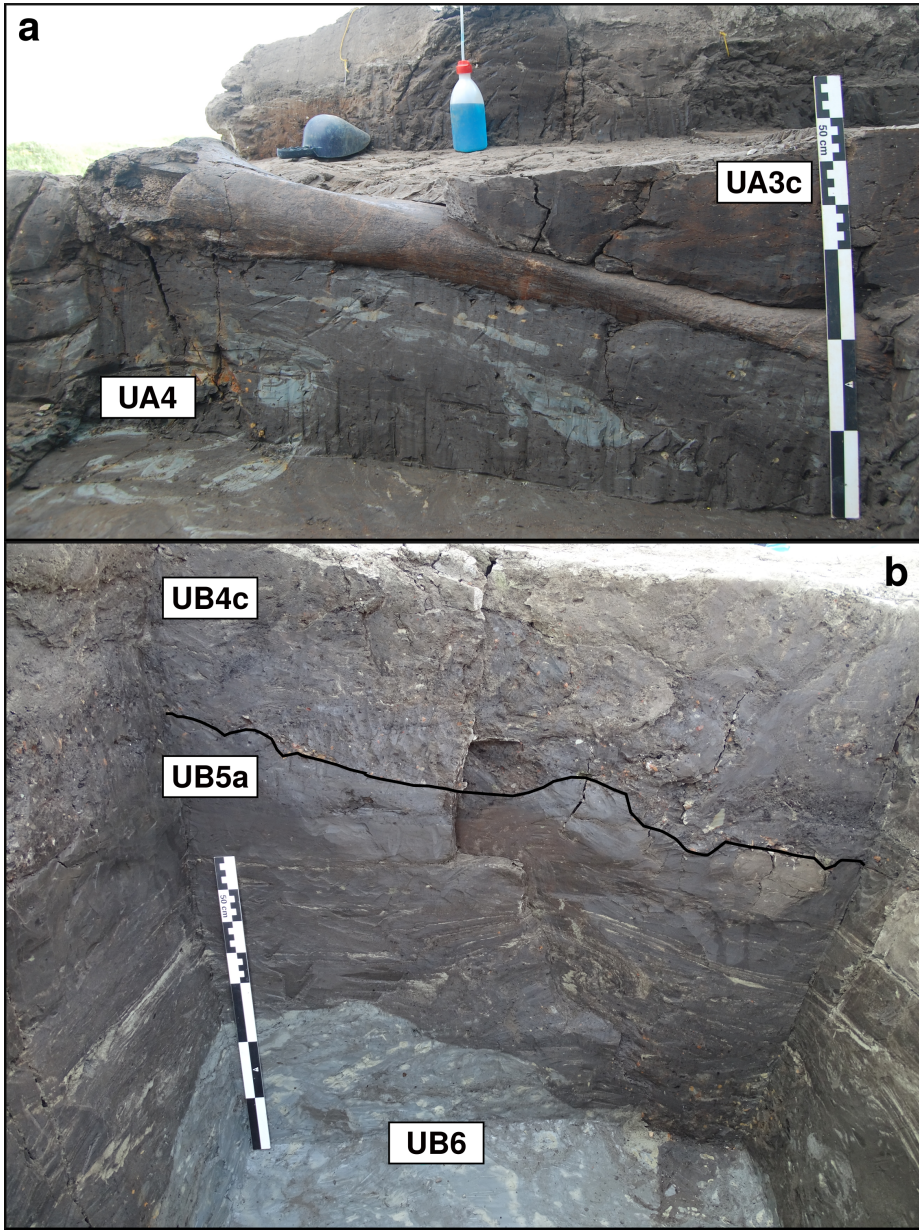


Figure 4: Photograph (2017) of the left femur of the *P. antiquus* skeleton, lying at the UA3c/4 contact and covered by unit UA3c (a). West profile (2014) of the excavation Area B (square 932/603), exposing the UB4c/5a (black solid line) and the UB5/6 erosional contacts (b).

104 tance. This model implies the loss of any original, pristine spatial relations between  
105 remains, but minor transport from the primary depositional *loci*. On the other hand, the  
106 allochthonous hypothesis (*sensu* Fernández-López, 1991; Domínguez-Rodrigo et al.,  
107 2012) implies significant transport from the original *loci* of deposition and re-elaboration  
108 (*sensu* Fernández-López, 1991). According to this model, the spurious spatial associa-  
109 tion between the lithic artefacts and faunal remains does not support any behavioural  
110 interpretation.

## 111 2. Material and methods

112 Since 2013, systematic investigation of the Marathousa 1 site has been carried out  
113 by a joint team from the Ephoreia of Palaeoanthropology-Speleology (Greek Ministry  
114 of Culture) and the University of Tübingen. A grid system of 1 square meter units  
115 was set up, oriented -14 degrees off the magnetic North, and including the two areas  
116 of investigation. The excavation of the deposit proceeded in 50x50 cm sub-squares in  
117 Area B and 1x1 m squares in Area A, and spits of 5 to 10 cm thickness, respectively.  
118 Systematic water-screening of sediments was carried out on-site using 1 mm sieves  
119 in order to guarantee recovery of the small-size fraction (e.g., micro-artefacts, small  
120 mammal remains, fish, molluscs and small fragments of organic and inorganic mate-  
121 rial). The three-dimensional coordinates of finds (i.e., all the lithic artefacts, teeth and  
122 diagnostic bones; bones and organic material with a-axis  $\geq 20$  mm), collected spits  
123 of sediment, samples and geological features (e.g., erosional contacts and mud cracks)  
124 were recorded with a total station. Specifically, the three-dimensional position of the  
125 finds was always recorded at the lowest point of contact of the item with the sediment.  
126 Dense clouds of surface points of the elephant skeletal elements were acquired using  
127 both a total station and a close-range photogrammetric technique.

128 The dimensions (length, width and thickness) of registered finds were measured  
129 on-site with millimetre rules. Orientation (plunge and bearing) of elongated particles  
130 (i.e., faunal remains, large wood fragments and lithic artefacts) was recorded since  
131 2013 using a clock-like system (the bearing was measured, relatively to the grid North,  
132 in twelve clockwise intervals of 30°; the plunge with a 22.5° accuracy). In 2015, the  
133 use of a compass and inclinometer with an accuracy of 1° was introduced in Area B to  
134 gradually replace the former method.

135 The widespread use of a compass and inclinometer to record orientation data (Voorhies,  
136 Fiorillo, 1991; Bertran and Texier, 1995; Bertran et al., 1997; Lenoble and  
137 Bertran, 2004; Eberth et al., 2007; Eren et al., 2010; Benito-Calvo et al., 2011; Domínguez-  
138 Rodrigo et al., 2012; Domínguez-Rodrigo and García-Pérez, 2013; Domínguez-Rodrigo  
139 et al., 2014c; Cobo-Sánchez et al., 2014; Organista et al., 2017, among others) was  
140 favoured over the alternative use of a total station (Kluskens, 1990; Dibble et al., 1997;  
141 McPherron, 2005; Enloe, 2006; Bernatchez, 2010, among others), mostly due to the  
142 time-restricted conditions of the rescue excavation conducted at Marathousa 1.

143 Measurements of the bearing (azimuth) and plunge (dip) of elongated finds were  
144 taken along the symmetrical longitudinal a-axis (SLA) of elongated bones (Domínguez-  
145 Rodrigo and García-Pérez, 2013), lithic artefacts (Bertran and Texier, 1995) and wood  
146 fragments (Macdonald and Jefferson, 1985), using the lowest endpoint of the a-axis as  
147 an indicator of the vector direction.

148 Other major axes have been alternatively used with the recent application of GIS  
149 techniques to retrieve orientation data from secondary source, i.e., from excavation  
150 photographs, drawings or maps (Boschian and Saccà, 2010; Benito-Calvo and de la  
151 Torre, 2011; de la Torre and Benito-Calvo, 2013; Walter and Trauth, 2013; García-  
152 Moreno et al., 2016; Sánchez-Romero et al., 2016). However, the experimental works  
153 of Domínguez-Rodrigo and García-Pérez (2013) and Domínguez-Rodrigo et al. (2014c)  
154 showed that the SLA, defined as the major axis which symmetrically divide the bone,  
155 is more accurate in estimating the flow direction, regardless of bone shape. This a-axis  
156 is widely used in taphonomic studies (Toots, 1965; Voorhies, 1969; Eberth et al., 2007;  
157 Domínguez-Rodrigo et al., 2012, 2014a; Aramendi et al., 2017, among others) for de-  
158 termining the preferential orientation of anisotropic assemblages. The a-axis or major  
159 axis of the artefact, measured as the long diameter of the triaxial ellipsoid that approx-  
160 imates the particle shape (Krumbein, 1941), is as well used in studies which employ a  
161 sedimentological approach to archaeological fabric (Bertran and Texier, 1995; Bertran  
162 et al., 1997; Lenoble and Bertran, 2004; Benito-Calvo et al., 2009, among others).

163 The present study focuses on the excavated stratigraphic units in which most of the  
164 archaeological and palaeontological remains were recovered in both excavation areas,  
165 namely in UA3c and UA4 in Area A, and UB4c and UB5a in Area B. From the total,  
166 subset samples of material were used for each specific spatial analysis. For the fabric  
167 analysis we included material collected until 2016. For the vertical distribution and  
168 point pattern analyses, the region of investigation was limited to the squares excavated  
169 from 2013 until 2015, 25 and 29 square meters respectively in each area (Fig. 2).

170 The analyses were performed in R statistical software (R Core Team, 2017). In  
171 order to make this research reproducible (Marwick, 2017; Marwick et al., 2017), a  
172 repository containing a compendium of data, source code and text is open licensed and  
173 available at the DOI: [10.5281/zenodo.822272](https://doi.org/10.5281/zenodo.822272)

### 174 2.1. Fabric analysis

175 The taphonomic study of the orientation pattern of elongated sedimentary particles,  
176 including bones and artefacts, first addressed by Voorhies (1969); Isaac (1967); Bar-  
177 Yosef and Tchernov (1972); Schick (1986), more recently led to a noteworthy develop-  
178 ment of methods and propagation of applications in Palaeolithic site formation studies  
179 (Bertran and Texier, 1995; Bertran et al., 1997; Lenoble and Bertran, 2004; Lenoble  
180 et al., 2008; McPherron, 2005; Benito-Calvo et al., 2009, 2011; Benito-Calvo and de la  
181 Torre, 2011; Bernatchez, 2010; Boschian and Saccà, 2010; Domínguez-Rodrigo et al.,  
182 2012; Domínguez-Rodrigo and García-Pérez, 2013; Domínguez-Rodrigo et al., 2014c;  
183 de la Torre and Benito-Calvo, 2013; Walter and Trauth, 2013; García-Moreno et al.,  
184 2016; Sánchez-Romero et al., 2016, among others).

185 Fabric analysis can provide valuable insight into site formation and taphonomic  
186 processes, allowing discrimination between different orientation patterns (isotropic,  
187 linear or planar) possibly associated with a range of sedimentary processes. Whereas  
188 water-flow deposits are generally characterised by relatively good sorting and preferred  
189 orientation of clasts parallel, or normal to the flow direction (linear fabric) (Petraglia  
190 and Potts, 1994); debris-flow deposits mostly exhibit massive, poorly bedded mixtures  
191 of unsorted sediments and random orientation of clasts (isotropic fabric), except at the

flow margins where linear fabric may occur (Pierson, 2005). On the other hand, undisturbed archaeological sites, as well as experimental assemblages, have been observed to have planar fabric (Bertran et al., 1997; Lenoble and Bertran, 2004). Nevertheless, grey zones exist between depositional processes, so that an unequivocal discrimination based only on fabric observations is often not possible, and other taphonomic criteria must also be considered (Lenoble and Bertran, 2004). As an example, while overland flows (runoff) have been observed to show some degree of planar fabric (Lenoble and Bertran, 2004), anisotropy without significant transport can be caused in a lacustrine floodplain by low-energy processes such as lake transgression and regression, as well as water-sheet flows formed during rainy seasons (Cobo-Sánchez et al., 2014).

At the margin of a lacustrine environment, relatively close to the surrounding relief, a combination of high- and low-energy processes can be expected. According to the sedimentological and micromorphological study of the Marathousa 1 site, the main find-bearing horizon is associated with hyperconcentrated flows (Karkanas et al., this issue). Hyperconcentrated flows are intermediate states, defined by sediment concentration, in the continuum between sub-aerial water flows and debris flows. Benvenuti and Martini (2002) reported that, when a turbulent hyperconcentrated flow expands over a surface - as in the case of Marathousa 1 - a two-phase flow may develop, with a more concentrated, coarser grained bottom flow-layer (traction carpet) moving slower than the upper turbulent flow-layer carrying wash-load and suspended load. Resultant deposit may exhibit diagnostic inverse grading, or a continuously aggrading bed. Parallel or normal orientation of the clasts to the flow direction can be observed (Benvenuti and Martini, 2002). A simulation model also showed that linear fabric can develop in mud flows. However, after deposition, settling of the clasts may affect the fabric to some extent, depending on the viscosity of the mud flow (Lindsay, 1968).

As part of our three-prong spatial analytic approach, we conducted comparative fabric analysis with the aim to investigate the dynamics of the depositional processes at Marathousa 1.

Since fabric strength has been found to be positively correlated with the shape and size of the clast, for the fabric analysis we subset samples of remains with length  $\geq 2$  cm and elongation index (the ratio length/width)  $I_e \geq 1.6$  (Lenoble and Bertran, 2004). The samples are listed in Table 1 and include mostly wood fragments and faunal remains from the four stratigraphic units under investigation. Bones have been found to readily react to water flow and show very early anisotropic patterns (Domínguez-Rodrigo et al., 2014c). Flume experiments showed that wood fragments as well tend to align parallel to the current direction (Macdonald and Jefferson, 1985). No distinction of skeletal elements was made, both due to the high fragmentation rate of faunal remains in Area B, and because recent experiments showed a similar orientation pattern for different bone shapes (Domínguez-Rodrigo et al., 2012; Domínguez-Rodrigo and García-Pérez, 2013).

The sample of bones belonging to the individual of *P. antiquus* from Area A was analysed separately and included the humerus, ulna, femur and tibia; the atlas, axis and other 16 complete vertebrae or vertebral fragments; 29 complete ribs or rib fragments; 2 calcanea; 4 metatarsals/metacarpals; the pyramidal; the trapezoid and the pelvis. The sample from UB5a was too small (only 7 observations) and was therefore excluded. In order to assess the reliability of the orientation data recorded using the clock method,

Table 1: List of sampled observations for the fabric analysis.

Sample	<i>n</i>	Type		
		Fauna	Wood	Lithic
UA3c	49	23	25	1
UA4	38	8	30	-
<i>P. antiquus</i>	63			
UB4c	38	30	1	7

we separately analysed two sub-samples from unit UB4c, selected from a set of finds recorded using both methods. All the sampled observations are representative of the whole study area.

Rose diagrams and uniformity tests, such as Rayleigh, Kuiper, Watson and Rao tests (Jammalamadaka et al., 2001), were used to visualise and evaluate circular isotropy in the sample distribution. The Rayleigh test is used to assess the significance of the sample mean resultant length ( $\bar{R}$ ), assuming that the distribution is unimodal and not bi- or plurimodal. The  $\bar{R}$  ranges from 0 to 1: values close to 1 indicate that the data are closely clustered around the mean direction; when the data are evenly spread  $\bar{R}$  has a value close to 0. A  $p$  – *value* lower than 0.05 rejects the hypothesis of uniformity with a 95% confidence interval. Kuiper, Watson and Rao are omnibus tests used to detect multimodal departures from circular uniformity. The Kuiper test (Kuiper, 1960) is a rotation-invariant Kolmogorov-Smirnov test statistic for testing the null hypothesis that the empirical distribution function fits a uniform distribution function. The Watson test (Watson, 1961) is instead related to the Cramer-von Mises test. The Rao's spacing test (Jammalamadaka et al., 2001) is based on the idea that in a uniform distribution successive observations should be approximately evenly spaced and it tests deviation from this distribution. For all the tests, results are evaluated against critical values: a result higher than the critical value rejects with confidence the null hypothesis. We applied three omnibus tests since none of them have very high power and some studies suggested that there is no test that is superior to the others under all circumstances (Pewsey et al., 2013).

Randomness testing of three-dimensional data was conducted with the Woodcock  $S_1/S_3$  test (Woodcock and Naylor, 1983). Considering both the plunge and bearing of the oriented items, this method, based on three ordered eigenvalues ( $S_1, S_2, S_3$ ), is able to discriminate the shape and strength of the distributions. The shape parameter  $K = \frac{\ln(S_1/S_2)}{\ln(S_2/S_3)}$  ranges from zero (uni-axial girdles) to infinite (uni-axial clusters). The parameter  $C = \ln(S_1/S_3)$  expresses the strength of the preferential orientation, and its significance is evaluated against critical values from simulated random samples of different sizes. A perfect random uniform distribution would have  $C = 0$  and  $K = 1$ .

The Benn diagram (Benn, 1994) adds to the Woodcock test an isotropy ( $IS = S_3/S_1$ ) and an elongation ( $ES = 1 - (S_2/S_1)$ ) index. Like the former method, it is able to differentiate between linear (cluster), planar (girdle) or isotropic distributions. There are no published raw data from actualistic studies on hyperconcentrated flows or other depositional processes affecting the orientation of bones and artefacts deposited on lacustrine floodplains (but see Morton (2004) and Cobo-Sánchez et al. (2014) as

Table 2: List of sampled observations for the vertical distribution and point pattern analyses.

Sample	<i>n</i>	Lithic class					Faunal class			
		Debris/chip	Flake	Bone flake	Tool	Core	Indet.	Bone	Tooth	Microfauna
UA3c	279	46	2	-	1	-	1	171	14	44
UA4	61	3	1	-	-	-	-	45	4	8
UB4c	1243	753	154	1	34	6	2	246	28	19
UB5a	101	50	12	-	3	-	-	30	3	3

pioneer studies on this subject). However, we included in the Benn diagram relevant references to published results from observation of fabrics in modern subaerial slope deposits, i.e., debris flow and runoff (Bertran et al., 1997; Lenoble and Bertran, 2004).

## 2.2. Vertical distribution

The vertical distribution of materials has been long investigated with the aim of identifying cultural levels, by visually interpreting cross-sectional plots. However, recent advances in GIS techniques allow to inspect at higher resolution the three-dimensional distributions of archaeological remains (McPherron et al., 2005; Anderson and Burke, 2008, among others).

In analysing the vertical dispersion of material at Marathousa 1, we provisionally assume that a general concentration of unsorted lithic artefacts and faunal remains in the proximity of the erosional surfaces would support an autochthonous origin of the assemblages; whereas a homogeneous vertical distribution of remains from the UA3c and UB4c units would suggest an allochthonous origin, significant transport and subsequent re-deposition of the material. Indeed, massive process such as hyperconcentrated flows, have high erosional power and rather chaotic structure, which may result in inverse or normal grading (Benvenuti and Martini, 2002).

In order to estimate the degree of vertical dispersion while controlling for the size of the archaeological material, dimensional classes were set up following typological criteria. Lithic artefacts were classified as debris/chips when smaller than a cutoff length of 15 mm (Tourloukis et al., this issue). Other classes include flakes, tools and cores; the latter being the bigger and heavier debitage product. Table 2 summarises the sample size for each class. Lithic debris/chips constitute the larger part of the assemblage from UB4c (60%) and UB5a (49%); whereas in Area A they represent only a moderate percentage in the upper UA3c unit (16%). The very rare presence of lithic artefacts in the underlying unit UA4 is nevertheless significant. In this unit, the faunal remains are also found in much lower numbers, their number reduced to one fourth of those found in UA3c. For the point pattern analysis (see below), we used the same subset of material for both excavation areas.

For Area B, the material recovered from the water-screening was randomly provenanced according to the 5 cm depth of the excavated spit and the coordinates of the 50x50 cm quadrant of the excavation square. Following the same excavation protocol, the same procedure was applied for the water-screened material of Area A, which was randomly provenanced according to 3D-coordinates of the 1x1 m excavation square and 10 cm spit.

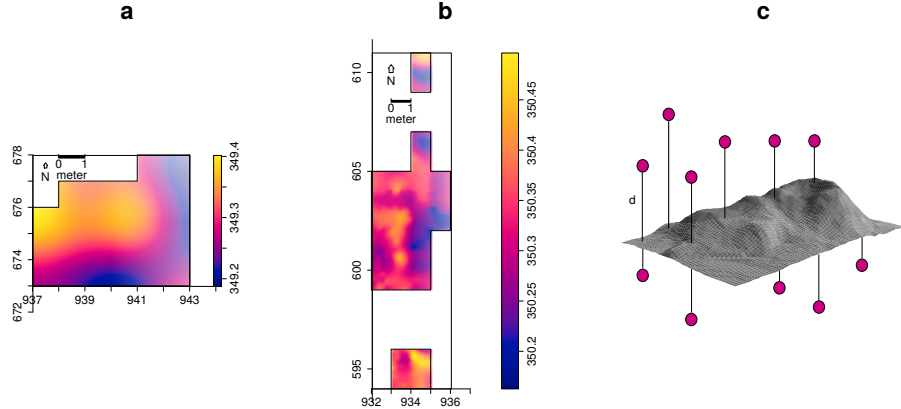


Figure 5: Ordinary Kriging interpolation of the UA3c/4 (a) and UB4c/5a (b) erosional surface; the colour scale denotes absolute elevation in m a.s.l. (c) Illustration of the method used to quantify the vertical dispersion of remains (d) with respect to the UA3c/4 (a) and UB4c/5a (b) surface.

Since the merely projection of points to virtual profiles is not a suitable method of analysis in presence of erosional, and thus uneven, geological contacts - such as those at Marathousa 1, ordinary Kriging interpolation of the recorded points of contact between the UA3c/UA4 and the UB4c/UB5a stratigraphic units were used to reconstruct the UA3c/4 and UB4c/5a erosional surfaces (Fig. 5a,b). In geostatistics, Kriging is a method of interpolation which, from a modelled function of spatial autocorrelation between known points (e.g., recorded elevations), calculates values of unknown points (e.g., predicted elevations). Thus, in order to address our specific objective, i.e., to quantify and analyse the vertical distribution of the archaeological and palaeontological material, we measured the minimum orthogonal distance ( $d$ ) of each specimen to the interpolated erosional surface (Fig. 5c). For the units above and below this surface (i.e., UB4c and UB5a), the relative distribution of lithic classes and faunal remains was informally tested by means of kernel density estimations.

In Area A, the UA3c/4 erosional contact is locally sharp, but, in contrast to Area B, parts of the eroded unit UA4 are mixed with pockets of the UA3c organic-rich silty sands and intraclast-rich mud flows (Karkanas et al., this issue). However, from sparse known points of the erosional contact, the UA3c/4 surface was interpolated and the vertical dispersion of remains estimated as well. The elephant remains were excluded from this analysis, since they clearly lie horizontally at the UA3c/4 contact (Fig. 4a).

Finally, a Student's two sample t-test allowed us to compare the empirical distributions of different groups of remains for each stratigraphic unit.

### 2.3. Point pattern analysis

A spatial point pattern is defined as the outcome of a random spatial point process (repetitions of it would always create a different pattern). The observed patterns of the archaeological and palaeontological remains were treated as manifestations of spatial point processes, i.e., site formation processes. Point pattern analysis investigates the

335 spatial arrangement of points with the aim of identifying spatial trends. In order to  
336 integrate the previous studies of the fabric and vertical distributions, we directed our  
337 point pattern analysis equally to the intensity of the patterns (the rate of occurrence of  
338 the recorded finds) and to the spatial interaction between different types of finds.

339 As the average number of random points per unit area, intensity informs about  
340 homogeneity or inhomogeneity in the distribution of events (e.g., clasts) generated by  
341 a point process (e.g., mud flow), i.e., whether the rate of occurrence is uniform or  
342 spatially varying across the study area. Intensity, usually non-parametrically evaluated  
343 by means of kernel density estimation ([Diggle, 1985](#)), was assessed for the distribution  
344 of material from the UB4c, UB5a and UA3c units. Cross-validation bandwidth, which  
345 assumes a Cox process, and edge correction were applied using the methods described  
346 in [Diggle \(1985\)](#).

347 In the presence of a covariate, it is recommended to further investigate the depen-  
348 dence of intensity on that explanatory variable ([Baddeley et al., 2012](#)). In order to  
349 evaluate whether variation in the density of materials was correlated to the topography  
350 of the erosional surface, we computed a local likelihood smoothing estimate of the in-  
351 tensity of remains from UB4c as a function of the UB4c/5a surface elevation model.  
352 Formal tests enabled us to assess the evidence of that dependence and to quantify the  
353 strength of the covariate. The Kolmogorov-Smirnov test of CSR (Complete Spatial  
354 Randomness) and Berman's  $Z_2$  statistics were used to test the strength of evidence for  
355 a covariate effect. The Receiver Operating Characteristic (ROC) plot, and the area  
356 under the ROC curve (AUC), closely related to Berman's  $Z_2$  test, measure the magni-  
357 tude of the covariate effect. AUC values close to 1 or 0 indicate strong discrimination,  
358 whereas intermediate values (0.5) suggest no discrimination power.

359 Intensity, evaluated by means of kernel density maps, although informative and  
360 widespread in the literature, nonetheless does not provide sufficient information to re-  
361 liably infer about site formation processes.

362 Whereas intensity is a first-order property of the point process, multiscale inter-  
363 point interaction is measured by second or higher-order moment quantities, such as the  
364 Ripley's  $K$  correlation function ([Ripley, 1976, 1977](#)) and the distance  $G$ -,  $F$ - and  $J$ -  
365 functions. Three different types of inter-point interaction are possible: random, regular  
366 or cluster. In a hypothesis-testing framework, point-wise envelopes are computed by  
367 a number of random simulations of the null hypothesis (i.e., random/Poisson distribu-  
368 tion). Thus, values of the empirical distribution (black solid line) are plotted against  
369 the benchmark value (red dotted line) and the envelopes (grey area) which specify the  
370 critical points for a Monte Carlo test ([Ripley, 1981](#)). Regular patterns are assumed to  
371 be the result of inhibition processes, while cluster patterns are the result of attraction  
372 processes.

373 In order to test the spatial interaction between remains associated with the erosional  
374 event of UB4c and those associated with the underlying UB5a unit, we treated the data  
375 as a multivariate point pattern, assuming that the point patterns in UB4c and UB5a are  
376 expressions of two different stationary point processes, i.e., depositional events. We  
377 performed a cross-type pair correlation function ( $g_{ij}(r)$ ), derivative of the multitype  
378  $K_{ij}(r)$  function, which is the expected number of points of type  $j$  lying at a distance  
379  $r$  of a typical point of type  $i$ . The function is a multiscale measurement of the spatial  
380 dependence between types  $i$  (UB4c) and  $j$  (UB5a). Randomly shifting in 199 Monte

381 Carlo permutations each of the two patterns, independently of each other, estimated  
382 values of  $\hat{g}_{ij}(r)$  are compared to a benchmark value  $g_{ij}(r) = 1$ , which is consistent with  
383 independence or at least with lack of correlation between the two point processes.

384 In addition to the pair correlation function, the multitype nearest-neighbour  $G_{ij}(r)$   
385 function was used to estimate the cumulative distribution of the distance from a point of  
386 type  $i$  (UB4c) to the nearest point of type  $j$  (UB5a). It measures the spatial association  
387 between the two assemblages. For the cross-type  $G$ -function, the null hypothesis states  
388 that the points of type  $j$  follow a Poisson (random) distribution in addition to being  
389 independent of the points of type  $i$ .

390 Thus, in a randomisation technique, when the solid line of the observed distribution  
391 ( $\hat{G}_{ij}(r)$  or  $\hat{g}_{ij}$ ) is above or below the shaded grey area, the pattern is significantly con-  
392 sistent with clustering or segregation, respectively. In order to reduce the edge effect  
393 bias in estimating the correlation between points, we implemented Ripley's isotropic  
394 edge correction (Ohser, 1983; Ripley, 1988).

395 Complete spatial randomness and independence (CSRI) of the two point processes  
396 (UB4c and UB5a) would support an allochthonous origin hypothesis for the assem-  
397 blage recovered from the UB4c unit. According to the allochthonous model, the mas-  
398 sive, chaotic UB4c flow event randomly re-elaborated the material entrained in it, inde-  
399 pendently from the material deposited in UB5a. On the other hand, positive or negative  
400 association can be interpreted as expressions of different autochthonous processes.

401 As for the three-dimensional distribution of the lithic artefacts in Area A, and  
402 their spatial association with the partial skeleton of the *P. antiquus*, we applied three-  
403 dimensional univariate and bivariate second-order functions. A rectangular box of 20  
404 square meters and 80 cm vertical extent was selected for the analyses (green outline in  
405 Fig. 11a). Assuming homogeneity, the univariate pair correlation function ( $g_3(r)$ ) was  
406 estimated for the pattern of all the artefacts (mostly debris/chips) from UA3c and UA4.

407 In the specific context of the site, complete spatial randomness (CSR) would sug-  
408 gest that the pattern most probably is the result of a random distribution process, such  
409 as a high energy mass movement, thus supporting an allochthonous model of depo-  
410 sition. On the other hand, spatial aggregation would support a primary origin of the  
411 assemblage. Nevertheless, topography and natural obstructions may generate spatial  
412 clustering as well.

413 In support to the pair correlation function, the cross-type nearest-neighbour func-  
414 tion has been applied in order to compute, for each artefact recovered from the UA3c  
415 and UA4 units, the nearest point of the three-dimensional clouds of points associated  
416 with the elephant skeleton. A prevalence of short distances would indicate aggregation  
417 of the lithic artefacts around the mass of the elephant; whereas a uniform or symmetric  
418 distribution would support the action of random independent processes.

### 419 3. Results

#### 420 3.1. Fabric analysis

421 The rose diagrams in Fig. 6 visualise the circular distributions of the examined  
422 specimens. Overall, the UA4 sample and the sample of elephant bones show uni-  
423 modal distributions with predominant peaks in the NE quadrant; while the ones from

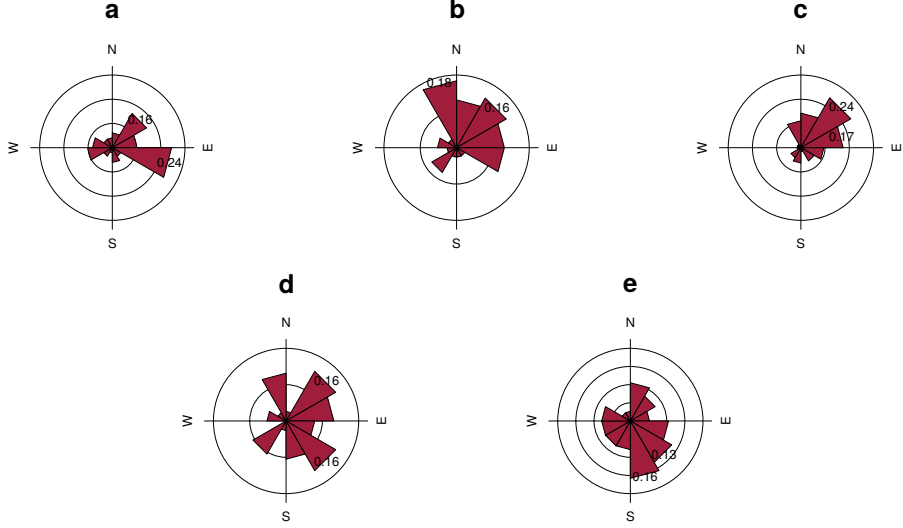


Figure 6: Rose diagrams showing the bearing patterns of samples from UA3c (a), UA4 (b), the elephant carcass (c) and UB4c (d: clock method, e: compass method).

Table 3: Value and  $p$  – value of circular uniformity test statistics.

Sample	mean dir.	Rayleigh		Kuiper		Watson		Rao	
		$\bar{R}$	$p$	$V_n$	$p$	$U^2$	$p$	$U$	$p$
UA3c	77.17°	0.268	0.029	2.4698	<0.01	0.2967	<0.01	271.8367	<0.001
UA4	35.79°	0.386	0.003	2.5656	<0.01	0.3437	<0.01	246.3158	<0.001
<i>P. antiquus</i>	54.64°	0.489	2.775e-07	3.4811	<0.01	0.906	<0.01	291.4286	<0.001
UB4c (clock)	91.66°	0.276	0.054	1.8963	0.01< $p$ <0.025	0.1937	0.025< $p$ <0.05	255.7895	<0.001
UB4c (compass)	151.17°	0.243	0.106	1.3944	>0.15	0.1268	>0.10	128.5263	>0.10

units UA3c and UB4c suggest multimodal distributions. Specifically, the UA4 sample distribution (Fig. 6b) spreads largely in the NE quadrant. Similarly, the circular distribution of the elephant sample (Fig. 6c), mainly lying in UA4, resembles the former distribution: it is skewed to the SW and concentrated in the NE quadrant. On the other hand, the UA3c sample (Fig. 6a) shows a bimodal distribution with two peaks to the E and NE, and the two samples from Area B (Fig. 6d,e) suggest a different multimodal scenario uniformly distributed.

Table 3 summarises the results of the circular uniformity tests. With regard to the UA3c sample, the Rayleigh test ( $p$  – value = 0.03) rejected the null hypothesis of circular uniformity. The mean resultant length ( $\bar{R} = 0.27$ ) and the mean direction of 77° are thus significant, assuming the distribution is unimodal. However, the rose diagram (Fig. 6a) showed a bimodal distribution. The Kuiper, Watson and Rao omnibus tests, more powerful than the Rayleigh test in detecting multimodal deviation from uniformity, also rejected the null hypothesis of uniformity, therefore suggesting significant anisotropy in the distribution.

For the UA4 sample and the subset of elephant bones, all the uniformity tests agreed in rejecting the null hypothesis in favour of a preferentially oriented distribution. The

441 elephant sample, with respect to the other, showed significantly higher test results, thus  
442 stronger anisotropy. As suggested by the rose diagrams (Fig. 6c), this sample has a  
443 mean direction towards the NE ( $55^\circ$ ) and relatively low circular variance ( $29^\circ$ ).

444 The UB4c sub-samples had discordant test results when considering the omnibus  
445 statistics. However, according to the Rayleigh test, the mean resultant lengths ( $\bar{R}$ )  
446 and the mean directions were not significant for both sub-samples of measurements:  
447  $p - values > 0.05$  failed to reject the null hypothesis of isotropy with 95% confidence  
448 interval. This result is well confirmed by the Kuiper, Watson and Rao tests for the  
449 sub-sample of measurements recorded using the compass. Conversely, the omnibus  
450 tests failed to reject the hypothesis of uniformity for the other sub-sample of measure-  
451 ments recorded with the clock method. The rose diagram (Fig. 6d) suggested for the  
452 latter distribution strong multimodality, with uniformly spread peaks. The contrasting  
453 results obtained for the UB4c sub-samples are most probably due to the shape of those  
454 distributions. Indeed, the clock system, being less accurate, tends to produce a less  
455 dense distribution, more subject to show a multimodal shape when the distribution is  
456 actually uniform.

457 The Woodcock eigenvalues ratio graph (Fig. 7a) presents the shape ( $K$ ) and strength  
458 ( $C$ ) of the distributions. Fig. 7b plots confidence levels of Monte-Carlo critical  $C$  val-  
459 ues, varying for sample sizes. The two sub-samples from Area B nearly overlapped,  
460 thus suggesting reliability of the orientation measurements collected using the clock  
461 system, although of low accuracy. The two sub-samples, together with the UA3c sam-  
462 ple, having low  $C$  values, plotted close to the origin of the ratio graph. Therefore, they  
463 indicate weak preferential orientation (UA3c) and significant randomness (UB4c). On  
464 the other hand, the UA4 and the elephant samples, with higher  $C$  values, showed a  
465 stronger and significant tendency to orient preferentially. The shape parameter  $K$  of  
466 the samples varied from  $K = 0.25$  for the UB4c sample measured with the compass,  
467 to  $K = 0.66$  for the one measured with the clock, to  $K = 0.48$  for the elephant sample.  
468 Overall, all the samples, except the UA3c one ( $K = 1.63$ ), plotted below the average  
469 shape value ( $K = 1$ ) between girdles and clusters distributions.

470 The Benn diagram (Fig. 8) resembles the Woodcock ratio graph (Fig. 7a). The  
471 samples from units UB4c and UA3c clearly plotted at a distance from the UA4 and  
472 the elephant samples. The UB4c samples plotted in the upper corner of the ternary  
473 graph, with the UB4c sub-sample of measurements taken with the compass exhibiting  
474 more isotropy. The UA3c sample, with an elongation index similar to the elephant  
475 sample, but higher isotropic index, plotted towards the centre. Compared to the ranges  
476 of fabrics recorded for modern natural processes (debris flow and runoff), the fabric  
477 from the UA3c and UB4c units plotted well inside the cluster of debris flows, with the  
478 UB4c (comp) sample suggesting even more random orientations. On the other hand,  
479 the sample of elephant remains, which lie mostly on UA4 and are covered by UA3c,  
480 plotted significantly close to the sample from unit UA4. They both presented the lowest  
481 isotropy index ( $IS$ ), but not high elongation index ( $EL$ ). Thus, they plotted in the  
482 average between linear and planar orientations, at the margins of the range of runoff  
483 processes. Yet they still plotted within the cluster of debris flows fabrics. Moreover,  
484 as suggested also by the uniformity tests (Tab. 3), the elephant sample showed a more  
485 linear attitude with respect to the UA4 sample.

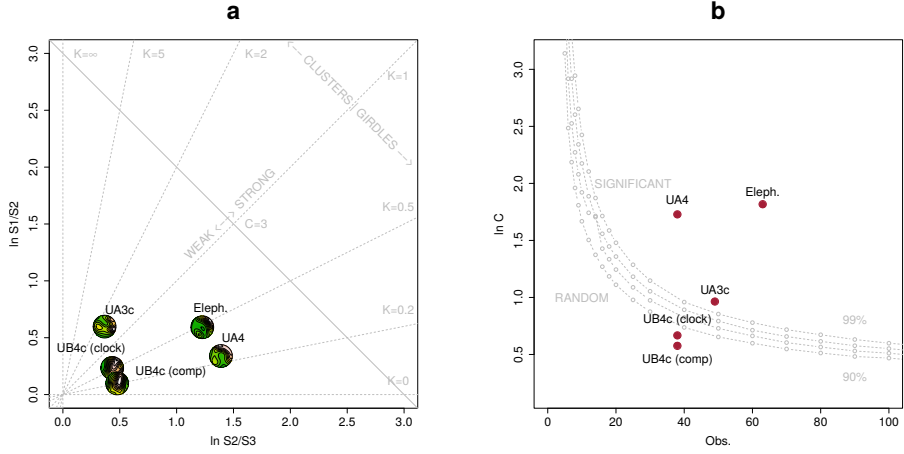


Figure 7: Woodcock's eigenvalues ratio graph (a) and plot of the Monte-Carlo critical  $S_1/S_3$  test values, for varying sample sizes and confidence levels (b), modified from [Woodcock and Naylor \(1983\)](#).

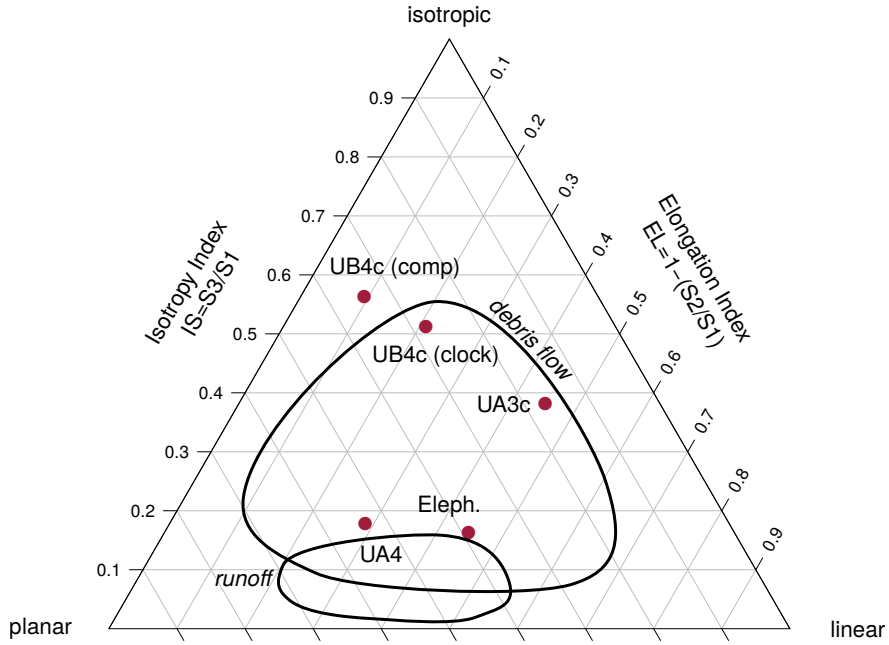


Figure 8: Benn's diagram. Fabric ranges of natural processes modified from [Lenoble and Bertran \(2004\)](#).

486     3.2. *Vertical distribution*

487     Fig. 9 compares the vertical distribution of the finds from units UA3c and UA4, by  
488 means of empirical density functions of the minimum distances ( $d$ ) from each speci-  
489 men to the UA3c/4 erosional contact (Fig. 5a). Three lithic artefacts (two flakes and  
490 one tool) from the UA3c unit, not included in Fig. 9, plotted within 15 cm from the  
491 interpolated surface. Only one flake has been found in the lower UA4, at about 17 cm  
492 from the UA3c/4 contact, together with three chips. Despite the scarcity of debitage  
493 products in this area, waste products (debris/chip) are relatively well represented (16%  
494 of the UA3c sample). Their vertical dispersion approximated a normal distribution  
495 ( $\mu = 0.24$ ,  $\sigma = 0.15$ ): the Kolmogorov-Smirnov and Shapiro tests failed to rejected  
496 the null hypothesis of normality ( $p - value = 0.83$  and 0.075, respectively). Notably, the  
497 distributions of the faunal remains from the same unit UA3c were all right skewed, with  
498 means ( $\mu$ ) about 20 cm above the UA3c/4 contact. Nevertheless, the Welch two sample  
499 t-test ( $p - value = 0.61$ ) failed to reject the null hypothesis that the lithic and faunal  
500 sample means are equal. The total distribution of remains from unit UA3c showed a  
501 unimodal distribution, skewed to the right, with mode in the proximity of the UA3c/4  
502 surface. Similarly, the vertical distribution of faunal remains recovered from unit UA4  
503 concentrate in the first 10 cm below surface. The density functions altogether clearly  
504 confirmed one of the main observations assessed during excavation, namely that, with  
505 the elephant remains lying at the UA3c/4 contact and covered by unit UA3c, most of the  
506 faunal and lithic material were recovered from unit UA3c (Fig. 2) and predominantly  
507 in the proximity of the UA3c/4 contact (Fig. 9).

508     Fig. 10 shows the empirical density functions of the minimum distances from each  
509 specimen from Area B to the UB4c/5a erosional contact (Fig. 5b). The combined  
510 distribution of any type of find from the UB5a unit (Fig. 10a) skewed to the left with  
511 a short tail (up to -0.3 m). The mode, between 5 and 10 cm below the roof of UB5a,  
512 indicates a general concentration of material very close to the contact of this unit with  
513 the overlying UB4c, in accordance with the mean distribution of the different classes of  
514 remains. Although the majority of both the lithic and faunal assemblages were found  
515 in the uppermost 15 cm of UB5a, few debris/chips and bone fragments occur lower  
516 in the sequence, yet no more than 30 cm below the roof of this unit. Very few flakes,  
517 three tools and no cores have been found in this unit. As a whole, the lithic assemblage  
518 from UB5a, mostly composed by debris/chips, is only 7% of the most conspicuous  
519 assemblage from UB4c.

520     The global distribution of unit UB4c was right skewed (up to almost 0.6 m) and  
521 centred at about 5 cm above the contact with the underlying unit UB5a (Fig. 10b).  
522 Almost 30% of the sample fell exactly at the erosional contact that separates UB4c  
523 from UB5a. The density estimations of the lithic debris/chip, flakes, tools and faunal  
524 remains significantly overlap, whereas the distribution of the six cores shows a bimodal  
525 shape with peaks at 5 and 20 cm above the contact. Moreover, the Welch Two Sample t-  
526 test of the lithic and faunal sample means failed to reject the null hypothesis ( $p-value =$   
527 0.6295).

528     3.3. *Point pattern analysis*

529     Results of the point pattern analysis are complementary to those obtained from the  
530 analysis of the fabric and vertical distributions.

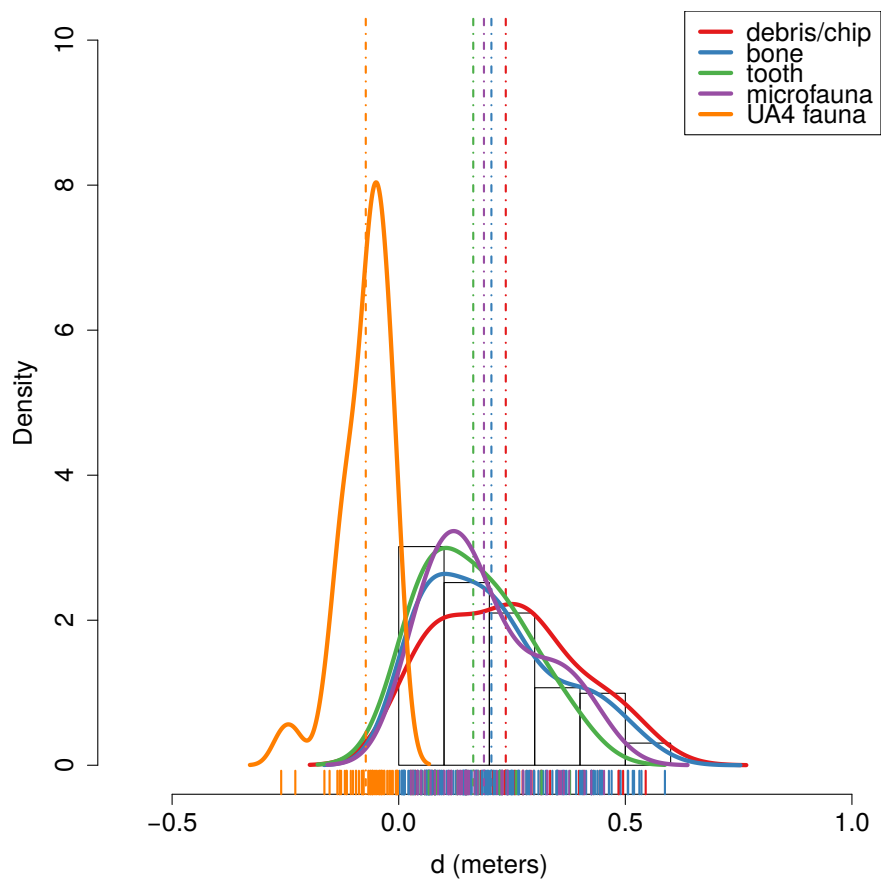


Figure 9: Empirical density functions of minimum orthogonal distances ( $d$ ) to the UA3c/4 surface. The histogram represents the total distribution of remains from UA3c; dashed lines indicate mean values.

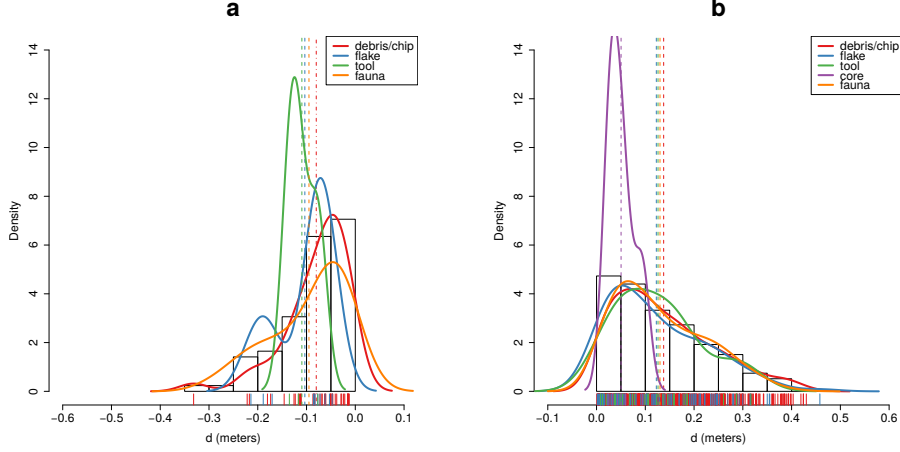


Figure 10: Empirical density functions of minimum orthogonal distances ( $d$ ) to the UB4c/5a surface. The histogram represents the total distribution of remains from UB5a (a) and UB4c (b); dashed lines indicate mean values.

531     Regarding Area A, kernel density estimation and three-dimensional functions were  
 532     applied in order to quantitatively depict the spatial distribution of the lithic assemblage  
 533     in relation to the elephant skeleton. Fig. 11a shows the smoothing kernel intensity  
 534     estimation of the faunal assemblage from the UA3c unit. Contour lines delimit the  
 535     density of the lithic sample. The partial skeleton of the *P. antiquus* is superimposed on  
 536     it. A preliminary visual examination of the plot suggests a homogeneous distribution  
 537     of lithics (mostly debris/chips) and fossils. Spots of higher density appear to be spread  
 538     around and in association with the elephant remains.

539     The univariate pair correlation function of the joined lithic assemblage from the  
 540     UA3c and UA4 units (Fig. 11b) suggests aggregation of finds. The estimated  $\hat{g}_3(r)$   
 541     function (black solid line) wanders above the benchmark value (red dotted line) until  
 542     values of  $r = 0.8$ . However, for distances between 35 and 65 cm, it lies above the  
 543     grey envelope of significance for the null hypothesis of CSR, indicating that at those  
 544     distances artefacts occur significantly closer than expected in the case of random pro-  
 545     cesses. For values of  $r > 0.8$ , the function stabilises at values close to 0, suggesting  
 546     a Poisson distribution. The plot illustrates the random distribution of finds between  
 547     patches of clusters that we observe in Fig. 11a.

548     The histogram in Fig. 11c shows the density of the distances calculated from each  
 549     artefact to the nearest-neighbour elephant remain. A right skewed distribution, with a  
 550     prevalent peak at 10 cm and mean ( $\mu$ ) 30 cm is an indication of the relatively strong  
 551     aggregation of lithics around the mass of the elephant skeleton.

552     As for Area B, the analysis focused on the spatial distribution and cross-correlation  
 553     of the assemblages from UB4c and UB5a. Figs. 12a,b respectively show kernel density  
 554     estimations of the combined lithic and faunal assemblages from both the units analysed.  
 555     Despite the samples size difference, a first visual examination suggests the presence of  
 556     interesting spatial structures.

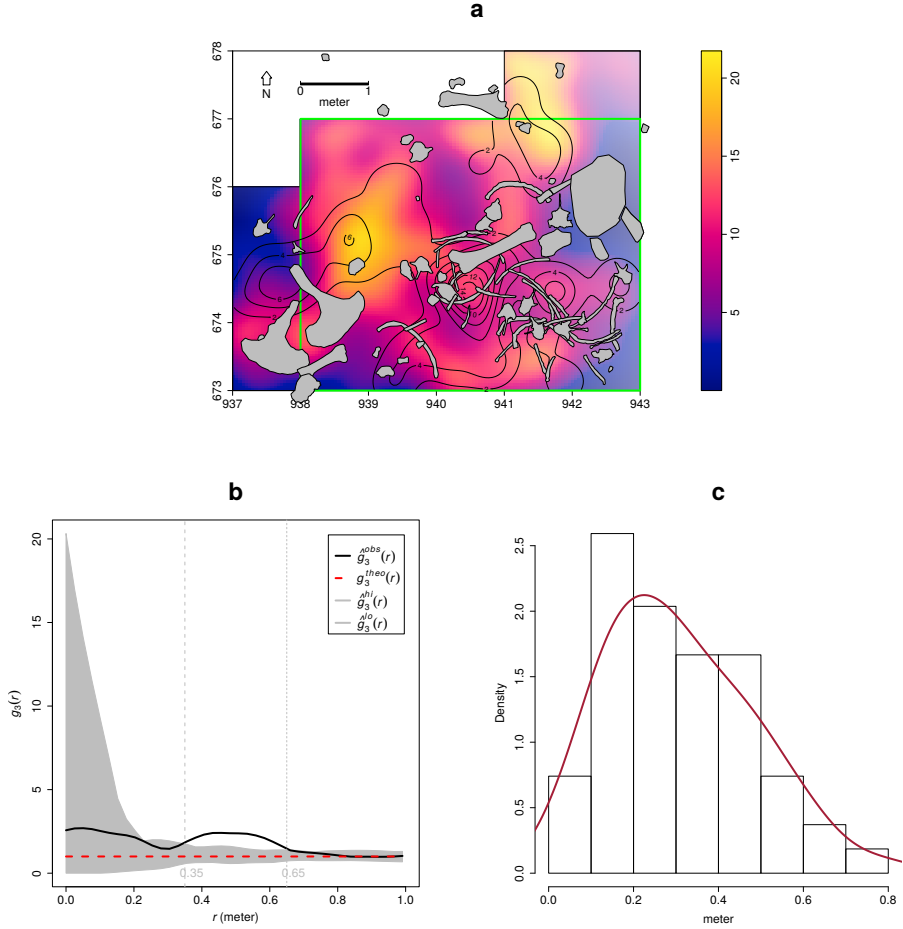


Figure 11: Kernel smoothed intensity function of the faunal assemblages from UA3c. Isolines mark the density of the lithic artefacts from UA3c (a). Pair correlation function ( $g_3(r)$ ) of a three-dimensional pattern of lithic artefacts from UA3c and UA4. Grey envelope of 999 Monte Carlo simulations under the CSR null hypothesis (b). Three-dimensional distance from each lithic artefact from UA3c and UA4 to the nearest neighbour elephant remain (c).

Regarding the UB4c unit (Fig. 12a), the high density of material concentrated around the western square 934/600 suggests that the pattern could have been the result of an inhomogeneous, non-uniform depositional process. Visual comparison of the density plot with the elevation model of the erosional contact between the UB4c and UB5a units (Fig. 5b) suggests positive correlation between lower elevations (topographic depressions) and higher density of remains. Fig. 12c shows the results of the  $\rho$ -function, which estimates the intensity of the UB4c sample assemblage as a function of the covariate underlying topography created by the erosional event. Within the range of elevation between 350.2 and 350.4 m, the occurrence of finds is higher and the intensity decreases with the rise of elevation, i.e., finds are more likely to be found at lower elevations than would be expected if the intensity was constant.

Spatial Kolmogorov-Smirnov (KS) and Berman's  $Z_2$  (Berman, 1986) statistics were used in order to test the dependence of the UB4c pattern on the covariate erosional surface. Both KS ( $D = 0.11952$ ,  $p - \text{value} = 7.772e - 16$ ) and  $Z_2$  ( $Z_2 = -7.8447$ ,  $p - \text{value} = 4.34e - 15$ ) significantly rejected the null hypothesis of CSR. Although the tests suggested evidence that the intensity depends on the covariate, the effect of the covariate is weak and it seems to have no discriminatory power. The ROC curve and AUC statistics (0.56), which measure the strength of the covariate effect, suggest that the underlying UB4c/5a topography does not completely explain the localised high density of occurrence in the UB4c.

Relative spatial segregation seems to occur between the assemblages from UB4c (Fig. 12a) and UB5a (Fig. 12b), with high density of the former distribution corresponding to low density of the latter. The former analysis of the vertical distribution showed that the two assemblages occur very close to their stratigraphic contact (Fig. 10). In order to further investigate the spatial interaction between the two depositional events, we applied multitype pair correlation ( $g_{ij}(r)$ ) and nearest-neighbour ( $G_{ij}(r)$ ) functions.

Fig. 12d shows the estimated values of the multivariate  $\hat{g}_{ij}(r)$  function against the envelope of the null hypothesis, obtained by randomly shifting the position of remains from the two distributions in 199 Monte Carlo simulations. For fixed values of  $r$  less than 30 cm the observed function lies below the benchmark value of independence, thus indicating segregation; but it wanders at the lower edge of the grey envelope. For fixed distances of  $r > 0.3$  m the observed and theoretical lines significantly overlap. Overall, the function suggests independence of the two point processes (UB4c and UB5a) at multiple scales.

However, the estimated  $\hat{G}_{ij}(r)$  function (Fig. 12c), running well below the significance grey envelope for fixed values of  $r > 0.3$  m, confirms that the nearest-neighbour distances between remains from UB4c and UB5a are significantly longer than expected in the case of independent processes. Interestingly, at values of  $r < 0.2$  m the observed function failed to reject the null hypothesis of Complete Spatial Randomness and Independence (CSRI).

#### 4. Discussion

Recent excavations at the Middle Pleistocene site of Marathousa 1 have unearthed in one of the two investigated areas (Area A) a partial skeleton of a single individual

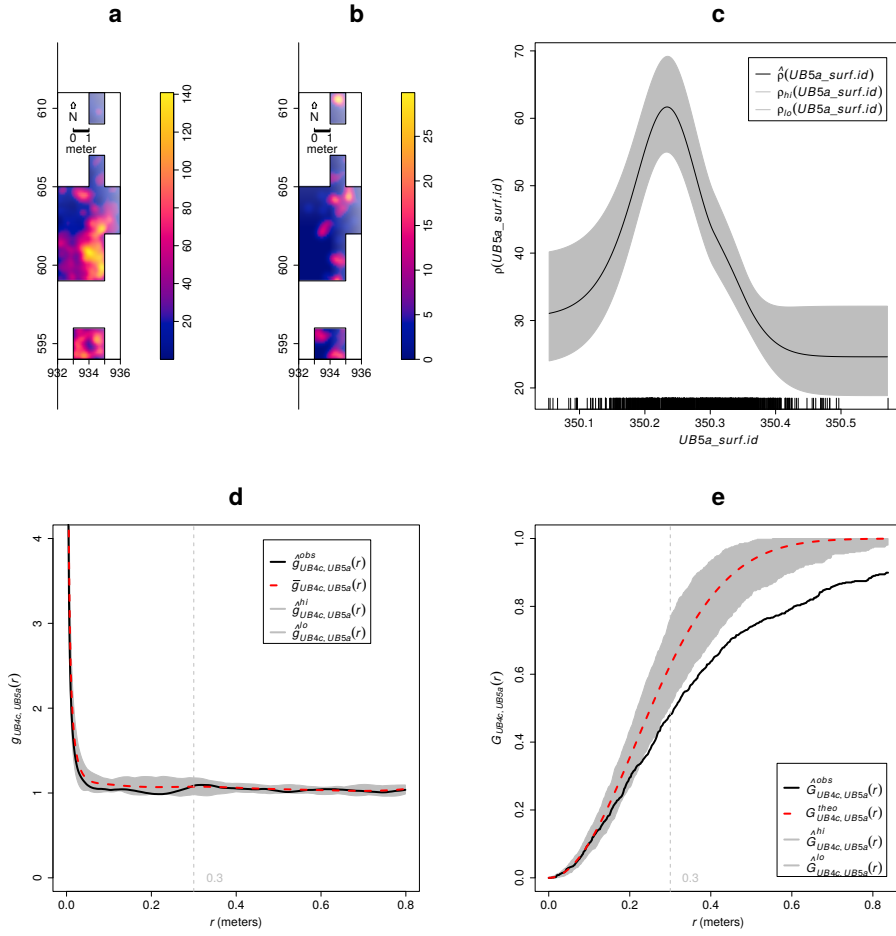


Figure 12: Kernel smoothed intensity function of the lithic and faunal assemblages from UB4c (a) and UB5a (b). Smoothing estimate of the intensity of remains from UB4c, as a function of the erosional surface UB4c/5a. Grey shading is point-wise 95% confidence bands (c). Cross-pattern pair correlation function ( $g_{ij}(r)$ ) between the UB4c and UB5a distributions. Grey envelope of 199 Monte Carlo simulations under the independence of components null hypothesis (d). Multitype nearest-neighbour function ( $G_{ij}(r)$ ) between the UB4c and UB5a distributions (e).

of *Palaeoloxodon antiquus*, whose bones are in close anatomical association, and spatially and stratigraphically associated with lithic artefacts and other faunal remains. In Area B, 60 m to the South of Area A, we collected a much higher number of lithic artefacts (Tourloukis et al., this issue), spatially and stratigraphically associated with other faunal remains, including isolated elephant bones, cervids and carnivores among others (Konidaris et al., this issue). The two areas are stratigraphically correlated, the main fossiliferous layers (UA3c and UB4c) representing a massive depositional process, such as a hyperconcentrated flow that dumped material in a lake margin context (Karkanas et al., this issue). To date, evidence of butchering (cut-marks) has been identified on two bones of the elephant skeleton from Area A, as well on elephant and other mammal bones from Area B (Konidaris et al., this issue).

However, due to the secondary depositional nature of the main fossiliferous horizon, it is of primary importance to evaluate the degree and reliability of the spatial association of the lithic artefacts with the faunal remains, and especially with the elephant skeleton. In order to tackle our main objective, we applied a comprehensive set of spatial statistics to the distributions of the archaeological and zooarchaeological/palaeontological remains from relevant stratigraphic units of the two areas of investigation. Preliminary results of our analyses are here discussed for both areas.

#### 4.1. Fabric analysis

The analysis of the orientation (plunge and bearing) of subsets of remains, mostly bone, wood fragments and lithic artefacts, showed different patterns for the two main find-bearing units.

In Area B, two sub-samples from the same stratigraphic unit were analysed, in order to assess the reliability of the orientation data measured with the clock system. Due to the different shapes of the distributions (Figs. 6d,e), test statistics reported contrasting results (Tab. 3). Indeed, the clock system, recording non-continuous circular data, tends to produce a distribution more subject to show a multimodal shape when it is actually uniform. However, the two sub-samples nearly overlapped when plotted in the three-dimensional Woodcock (Fig. 7) and Benn (Fig. 8) diagrams, thus suggesting some degree of reliability of the clock method. Nevertheless, despite minor differences between the two samples, caution should be paid in analysing grouped circular data.

The test results (Tab. 3) for the UA4 sample and the sample of elephant remains - which lie on unit UA4 and are covered by UA3c - indicated significant preferential orientations towards the NE (Figs. 6b,c). As shown by the Woodcock's (Fig. 7) and the Benn's diagrams (Fig. 8), these samples plotted together at a distance from the others. Such convergence suggests that the elephant carcass, the other faunal remains and the organic material, deposited on unit UA4, were subject to the same processes.

Far from the isotropic corner in the Benn's diagram these two samples from Area A plotted approximately in between the linear and planar extremes, with the elephant sample showing a more linear fabric. When the results published by Bertran et al. (1997) and Lenoble and Bertran (2004) from observations of fabrics in modern sub-aerial slope deposits were used as a reference, the two samples aggregated at the extreme margins of runoff processes. Yet, they plotted well within the cluster of debris flows and relatively distant from the linear corner.

645 Although Bertran et al. (1997) studied runoff deposits from different environments  
646 (channel-lag gravels in rills, small gullies, and inter-rill surfaces on alpine slopes; and  
647 faintly laminated gravel lenses on an inactive, small colluvial fan), this result is consist-  
648 ent with the exposure of unit UA4 to overland water-laden processes that occurred be-  
649 fore the flood event UA3c/UB4c. Notably, the erosive nature of low-energy processes  
650 triggered by rain-water has been observed on lacustrine floodplains, and is associated  
651 with anisotropic patterns in autochthonous assemblages (Cobo-Sánchez et al., 2014;  
652 Domínguez-Rodrigo et al., 2014c; García-Moreno et al., 2016).

653 Pockets of thinly bedded organic-rich silty sands have been found mixed in UA4.  
654 These sands in Area A resemble the UB5b/c sandy deposit in Area B, which is associ-  
655 ated with relatively high energy fluvial flows entering the lake margins (Karkanas et al.,  
656 this issue). Eventually, such relatively high energy flood (UB5b/c) would have had the  
657 power to significantly reorient elements of the elephant carcass and slightly displace  
658 them. However, the elephant skeleton clearly lies on top of unit UA4 and is covered by  
659 UA3c (see Fig. 4).

660 Moreover, unlike bones with a tubular shape (i.e., long bones), ribs and vertebrae  
661 are prone to orient preferentially under high energy processes, less likely under low  
662 energy processes (Domínguez-Rodrigo and García-Pérez, 2013; Domínguez-Rodrigo  
663 et al., 2014c). Interestingly, whereas some of the ribs share the same preferential orien-  
664 tation with the long bones, others are oriented NW/SE. However, a NW/SE orientation  
665 could be consistent with a prevalent NE direction of the flow (and vice-versa), since  
666 long bones could roll orthogonally to the flow direction (Voorhees, 1969). On the other  
667 hand, a higher energy flood would lead to an under-representation of skeletal elements  
668 with FTI (Fluvial transport Index) values  $\geq 75$  (sacrum, patella, astragalus, calcaneum,  
669 cervical, thoracic and lumbar vertebrae), which are more prone - when disarticulated  
670 - to be easily transported by water induced processes (Frison and Todd, 1986). Yet,  
671 several of these bones are present and in close spatial association with the elephant  
672 cranium and other skeletal elements. The presence of many of the skeletal elements  
673 with different transportation properties suggests that the elephant carcass was not sub-  
674 jected to high energy processes (and probably still articulated) before the flood event  
675 UA3c/UB4c.

676 The fabrics of the UA3c and UB4c samples, with higher isotropic index (*IS*), plotted  
677 at a significant distance from the elephant sample, yet within the cluster of debris  
678 flows (Fig. 8). Indeed, random distribution and orientation of clasts is expected for de-  
679 bris flows, except at flow margins, where preferential orientation and clusters of clasts  
680 have been observed (Pierson, 2005). However, hyperconcentrated flows, such as the  
681 UA3c/UB4c flood event, which fall in between the spectrum of water and debris flows,  
682 may develop parallel or normal orientation to the flow direction (Lindsay, 1968; Ben-  
683 venuti and Martini, 2002). Notably, with respect to the UB4c sample, the UA3c sample  
684 exhibits a higher elongation index (*ES*), similar to that of the elephant sample (Fig. 8).  
685 Rose diagrams (Fig. 6) and uniformity tests (Tab. 3) also suggest similar fabrics of the  
686 samples from Area A.

687 Thus, we can assume that an overland flow, namely UA3c/UB4c, is likely to have  
688 slightly reworked and preferentially oriented to the NE the exposed elements of the  
689 already dismembered (and probably already marginally displaced) elephant carcass,  
690 which mostly preserves close anatomical associations, but not anatomical connections.

691 Although little is currently known about the spatial extension of the UA3c/UB4c  
692 flow event, the different orientation patterns between the two areas could probably  
693 be explained with lateral variability. Indeed, the same event could exhibit different  
694 behaviours at different temporal and spatial points, giving rise to different distribution  
695 patterns.

696 As suggested by [Lenoble and Bertran \(2004\)](#), fabric analysis is not sufficient to un-  
697 equivocally discriminate processes and should therefore be integrated with the analysis  
698 of other diagnostic features.

#### 699 4.2. Vertical distribution

700 As for the vertical distribution, we assumed that mass processes, such as hypercon-  
701 centrated flows, would predominantly distribute poor to very poor sorted clasts homo-  
702 geneously throughout the sequence ([Pierson, 2005](#)). Diagnostic inverse grading, or a  
703 continuously aggrading bed can be observed in the resultant deposits ([Benvenuti and  
704 Martini, 2002](#)). A concentration of unsorted elements in the proximity of the erosional  
705 surface, as well as the absence of any grading, would in turn suggest an autochthonous  
706 assemblage.

707 The lithic assemblage from Area A - the combined units UA3c and UA4 ( $n = 54$ ),  
708 composed by a fewdebitage products and a relatively high number of debris/chips  
709 and retouch waste products ([Tab. 2](#)) - plotted predominantly in the proximity of the  
710 erosional surface created by the UA3c/UB4c event ([Fig. 5a](#)). The faunal remains from  
711 unit UA3c resemble the distribution of the archaeological assemblage; whereas the  
712 ones from the underlying unit UA4 plotted within 10 cm below the erosional contact.  
713 Overall, the material recovered from unit UA3c did not show any grading and mainly  
714 plotted at the bottom of the unit ([Fig. 9](#)). Thus, its vertical distribution is consistent  
715 with the hypothesis of an autochthonous assemblage.

716 In Area B, two samples from units UB4c ( $n = 1243$ ) and UB5a ( $n = 101$ ) respec-  
717 tively, were analysed ([Tab. 2](#)) for quantifying the minimum orthogonal distance of each  
718 item to the modelled erosional surface ([Fig. 5b](#)).

719 The vertical distribution of lithic artefacts and fossils from unit UB4c showed a pre-  
720 dominant peak right at the contact with the erosional surface. Almost 30% of this rich  
721 sample plotted at a distance between 0 and 5 cm from the erosional contact; whereas  
722 the rest gently skewed to the upper part of the unit, up to about 50 cm. The same distri-  
723 bution was observed for all classes of remains, suggesting no size sorting and an origin  
724 very close to the erosional surface ([Fig. 10b](#)).

725 The density distribution of the sample from the underlying UB5a unit ([Fig. 10a](#))  
726 globally indicates a more constrained vertical displacement of remains (within 30 cm  
727 below the erosional surface). Whereas lithic artefacts and fossils mostly plot right at  
728 the contact and just below it, a few debris/chips and faunal remains were found lower  
729 in the sequence. No size sorting was observed, but, notably, lithic cores are absent and  
730 the debris/chip distribution is wider than the distribution of the few flakes and tools.

731 Field observations of cracks in the clayey UB5a unit testify to shrinking and swelling  
732 during wet and dry cycles ([Karkanas et al., this issue](#)), which suggests that vertical dis-  
733 placement of some small lithics and fossil fragments at lower depths with respect to  
734 the UB5a/4c contact probably resulted from clay desiccation.

Likewise, [Lenoble and Bertran \(2004\)](#) documented up to 30 cm vertical dispersion and frequent vertical plunge of artefacts from the marshy silty clay of the Croix-de-Canard site, sector 3. Furthermore, a recent experimental study of animal trampling in water saturated substrates reported negative correlation with artefact size, significant inclination and greater vertical displacement than any former work: a maximum between 16 and 21 cm, with a mean of about 6 cm ([Eren et al., 2010](#)).

The fact that the majority of the remains from units UB4c and UB5a plotted at, or very close to the contact between these two layers, the relatively high percentage of lithics in both units, as well as the absence of grading, suggest autochthonous assemblages, deposited in UB5a and subsequently eroded *in situ* by the UA3c/UB4c flood event.

#### 4.3. Point pattern analysis

The autochthonous hypothesis was further explored by means of point pattern analysis. According to this model, in both areas the lithic and faunal assemblages were primarily deposited *in situ* and were subsequently eroded and re-deposited (*sensu* [Fernández-López, 1991](#)) by the hyperconcentrated flow UA3c/UB4c. We assumed that a completely random spatial distribution of the lithic artefacts and faunal remains would suggest an allochthonous origin and subsequent re-elaboration (*sensu* [Fernández-López, 1991](#)), with transport to the site by the action of a random massive process. Nevertheless, clustering of artefacts is not necessarily evidence of human presence. Aggregation or segregation patterns could be produced by a range of biotic and/or natural processes. Human activities, topography and physical obstructions alike could trigger spatial aggregation.

The three-dimensional distribution of lithic artefacts from unit UA3c shows significant clustering for values of  $r$  between 35 and 65 cm. Lithic artefacts occur relatively close to the skeletal elements of the elephant, at a distance between 20 and 50 cm at most (Fig. 11). The richest cluster of about 20 lithic artefacts is located to the SW of the cranium, close to the right femur and the scatter of ribs and vertebrae.

Considering the prevalent NE orientation of the elephant bones and the other faunal remains from UA4 and UA3c, it is not unlikely that a SW/NE oriented flood could have been responsible for the observed accumulation to the SW of the elephant cranium, which would have represented an important obstruction to the flow. A similar case of clustering of small remains, apparently dammed by a long elephant tusk, has also been observed at Castel di Guido (Italy) by [Boschian and Saccà \(2010\)](#). Secondary deposition by low-energy flows and clustering of artefacts and bones blocked by an aurochs carcass have been as well documented at the site of 'Ein Qashish (Israel) ([Hovers et al., 2014](#)).

However, the pair correlation function (Fig. 9b) suggests significant clustering of lithic artefacts at relatively small scale: a pattern less likely to be produced by a large scale massive process such as a hyperconcentrated flow. Moreover, clusters of lithic artefacts occur as well in areas with lower densities of elephant bones.

Small scale clustering; proximity to the elephant remains and the erosional surface; absence of spatial size sorting and, on the contrary, the presence of a relatively high number of lithic debris/chips associated with some flakes, tools and a rich faunal assemblage; close anatomical spatial association of the elephant skeletal elements,

780 slightly displaced and preferentially oriented: altogether these lines of evidence support  
781 the hypothesis of an autochthonous deposition, subject to localised minor reworking.

782 A similar pattern can be observed in Area B, where an initial set of spatial statistics  
783 confirmed that the inhomogeneous density of remains from unit UB4c (Fig. 12a) is  
784 not completely explained by the covariate effect of the underlying complex topography  
785 created by the erosional event UA3c/UB4c (Fig. 5b).

786 Thus, we explored the relative spatial interaction between the UB4c and the un-  
787 derlying UB5a samples. We assumed that complete spatial randomness of the two  
788 independent depositional processes would occur in case of an allochthonous origin and  
789 transportation of the UB4c assemblage. The hypothesis of an autochthonous original  
790 deposition of the faunal and lithic assemblages on the UB5a unit, subsequently eroded  
791 *in situ* by a relatively high energy flood (UB4c), was tested by cross-pattern spatial  
792 correlation functions (Figs. 12d,e). Whereas the two samples are vertically adjacent to  
793 the erosional surface (Fig. 10), on the horizontal plane they are both more segregated  
794 than expected for a random distribution.

795 Conversely, the extraordinary preservation and number of mint to sharp, unsorted  
796 lithic artefacts from the UB4c unit; their density, positively correlated to the topog-  
797 raphy, and significantly segregated from the underlying distribution of remains; the  
798 vertical proximity of both assemblages from UB4c and UB5a to the erosional surface;  
799 as well as the random orientation pattern of the former, suggest that significant dis-  
800 placement of materials due to the erosional event can be excluded.

801 The faunal and lithic assemblages from unit UB4c therefore most likely derived  
802 from the local erosion of exposed mudflat areas (unit UB5a) and have been slightly  
803 redistributed by the same flood event that capped the elephant in Area A.

804 Further evidence that the recovered assemblage has not undergone substantial re-  
805 working and has retained its original characteristics would come from the refitting anal-  
806 ysis, currently in progress. To date, 4 bone refits have been found in Area B: three from  
807 unit UB4c, respectively at 4.77, 0.05 and 0.01 m distance; and one between two mam-  
808 mal bone fragments from units UB4c and UB5a, at a very short distance (0.09 m).  
809 Interestingly, one of the elements of the most distant refit (a *Dama* sp. mandibular  
810 fragment) shows traces of carnivore gnawing ([Konidaris et al., this issue](#)).

811 In conclusion, multiple lines of evidence reject an allochthonous hypothesis of de-  
812 position in favour of an autochthonous model. The erosional event UA3c/UB4c repre-  
813 sents an *en masse* depositional process, i.e. a hyperconcentrated flow, in the continuum  
814 between water and debris flow, which would have locally reworked at a small scale  
815 the already exposed or slightly buried and spatially associated lithic and faunal assem-  
816 blages.

817 Although the UA3c/UB4c process represents a snapshot of a relatively short time-  
818 frame, high resolution inferences about the use of space by human groups, in terms  
819 of knapping episodes and butchering activities, are unreliable in light of the current  
820 information.

821 The spatial pattern observed at the site is indeed the result of the last episode in a  
822 palimpsest of spatial processes. Whereas the erosional event represented by the hyper-  
823 concentrated flow UA3c/UB4c caps the fossiliferous horizon and preserves the record,  
824 little is known about the underlying, eroded 'occupational' surface.

825 However, whereas hunting or scavenging in the Lower Palaeolithic is still an un-

826 solved matter of debate, considering the rate of bone fragmentation, the density of lithic  
827 debris/chips, the number of processed bones and their spatial density and association, it  
828 is likely that the assemblage represents a complex palimpsest of locally repeated events  
829 of hunting/scavenging and exploitation of lake shore resources.

830 More data from high resolution excavations in the coming years will allow us to  
831 refine the coarse-grained spatio-temporal resolution of our inferences about past human  
832 behaviour at Marathousa 1.

## 833 **5. Conclusions**

834 At the Middle Pleistocene open-air site of Marathousa 1, a partial skeleton of a  
835 single individual of *Palaeoloxodon antiquus* was recovered in stratigraphic association  
836 with a rich and consistent lithic assemblage and other vertebrate remains. Cut-marks  
837 and percussion marks have been identified on the elephant and other mammal bones ex-  
838 cavated at the site. The main find-bearing horizon represents a secondary depositional  
839 process in a lake margin context.

840 Understanding the site formation processes is of primary importance in order to  
841 reliably infer hominin exploitation of the elephant carcass and other animals. To meet  
842 this aim, we applied a comprehensive set of multivariate and multiscale spatial analyses  
843 in a taphonomic framework.

844 Results from the fabric, vertical distribution and point pattern analyses are consis-  
845 tent with a high-energy erosional process, such as a hyperconcentrated flow deposited  
846 at the margin of a swamp, reworking at a small scale an exposed (or slightly buried) and  
847 consistent scatter of lithic artefacts and faunal remains. These results are in agreement  
848 with preliminary taphonomic observations of the lithic artefacts ([Tourloukis et al., this issue](#))  
849 and the faunal remains ([Konidaris et al., this issue](#)), which also indicate minor  
850 weathering and transportation. Our analyses show that multiple lines of evidence sup-  
851 port an autochthonous origin of the lithic and faunal assemblages, subject to minor  
852 post-depositional reworking.

## 853 **Acknowledgements**

854 This research is supported by the European Research Council (ERC StG PaGE  
855 283503) awarded to K. Harvati. We are grateful to the Municipality of Megalopolis,  
856 the authorities of the Region of Peloponnese, and the Greek Public Power corpora-  
857 tion (ΔΕΗ) for their support. We also thank Julian Bega and all the participants in the  
858 PaGE survey and excavation campaigns in Megalopolis for their indispensable coop-  
859 eration. We are grateful to the editors and two anonymous reviewers for their critical  
860 discussions and many constructive comments that helped to improve this manuscript.

## 861 **References**

- 862 Anderson, K. L., Burke, A., 2008. Refining the definition of cultural levels at Karabi  
863 Tamchin: a quantitative approach to vertical intra-site spatial analysis. *Journal of*  
864 *Archaeological Science* 35 (8), 2274–2285.

- 865 Aramendi, J., Uribelarrea, D., Arriaza, M. C., Arráiz, H., Barboni, D., Yravedra, J.,  
866 Ortega, M. C., Gidna, A., Mabulla, A., Baquedano, E., Domínguez-Rodrigo, M.,  
867 2017. The paleoecology and taphonomy of AMK (Bed I, Olduvai Gorge) and its  
868 contributions to the understanding of the “Zinj” paleolandscape. *Palaeogeography,  
869 Palaeoclimatology, Palaeoecology* (in press).
- 870 Baddeley, A., Chang, Y.-M., Song, Y., Turner, R., 2012. Nonparametric estimation of  
871 the dependence of a point process on spatial covariates. *Statistics and Its Interface*  
872 5 (2), 221–236.
- 873 Bailey, G., 2007. Time perspectives, palimpsests and the archaeology of time. *Journal  
874 of Anthropological Archaeology* 26 (2), 198–223.
- 875 Bar-Yosef, O., Tchernov, E., 1972. On the palaeo-ecological history of the site of Ubei-  
876 diya. Vol. 35. Israel Academy of Sciences and Humanities, Jerusalem.
- 877 Bargalló, A., Gabucio, M. J., Rivals, F., 2016. Puzzling out a palimpsest: Testing an  
878 interdisciplinary study in level O of Abric Romaní. *Quaternary International* 417,  
879 51–65.
- 880 Benito-Calvo, A., de la Torre, I., 2011. Analysis of orientation patterns in Olduvai  
881 Bed I assemblages using GIS techniques: Implications for site formation processes.  
882 *Journal of Human Evolution* 61 (1), 50–60.
- 883 Benito-Calvo, A., Martínez-Moreno, J., Mora, R., Roy, M., Roda, X., 2011. Trampling  
884 experiments at Cova Gran de Santa Linya, Pre-Pyrenees, Spain: their relevance for  
885 archaeological fabrics of the Upper–Middle Paleolithic assemblages. *Journal of Ar-  
886 chaeological Science* 38 (12), 3652–3661.
- 887 Benito-Calvo, A., Martínez-Moreno, J., Pardo, J. F. J., de la Torre, I., Torcal, R. M.,  
888 2009. Sedimentological and archaeological fabrics in Palaeolithic levels of the  
889 South-Eastern Pyrenees: Cova Gran and Roca del Bous Sites (Lleida, Spain). *Jour-  
890 nal of Archaeological Science* 36 (11), 2566–2577.
- 891 Benn, D., 1994. Fabric shape and the interpretation of sedimentary fabric data. *Journal  
892 of Sedimentary Research* 64 (4a), 910–915.
- 893 Benvenuti, M., Martini, I. P., 2002. Analysis of terrestrial hyperconcentrated flows and  
894 their deposit. In: Martini, I. P., Baker, V. R., Garzón, G. (Eds.), *Flood and Megaflood  
895 Processes and Deposits*. Vol. 32 of Special Publication of the International Associa-  
896 tion of Sedimentologists. Blackwell Publishing Ltd., pp. 167–193.
- 897 Berman, M., 1986. Testing for spatial association between a point process and another  
898 stochastic process. *Applied Statistics* 35, 54–62.
- 899 Bernatchez, J. A., 2010. Taphonomic implications of orientation of plotted finds from  
900 Pinnacle Point 13B (Mossel Bay, Western Cape Province, South Africa). *Journal of  
901 Human Evolution* 59 (3–4), 274–288.

- 902 Bertran, P., Hetù, B., Texier, J.-P., Steijn, H. V., 1997. Fabric characteristics of subaerial  
903 slope deposits. *Sedimentology* 44 (1), 1–16.
- 904 Bertran, P., Texier, J.-P., 1995. Fabric Analysis: Application to Paleolithic Sites. *Journal*  
905 of Archaeological Science 22 (4), 521–535.
- 906 Bevan, A., Crema, E., Li, X., Palmisano, A., 2013. Intensities, Interactions, and Un-  
907 certainties: Some New Approaches to Archaeological Distributions. In: Bevan, A.,  
908 Lake, M. (Eds.), Computational Approaches to Archaeological Spaces. Left Coast  
909 Press, Walnut Creek, pp. 27–52.
- 910 Binford, L. R., 1981. Behavioral Archaeology and the "Pompeii Premise". *Journal of*  
911 *Anthropological Research* 37 (3), 195–208.
- 912 Boschian, G., Saccà, D., 2010. Ambiguities in human and elephant interactions? Sto-  
913 ries of bones, sand and water from Castel di Guido (Italy). *Quaternary International*  
914 214 (1–2), 3–16.
- 915 Brantingham, P. J., Surovell, T. A., Waguespack, N. M., 2007. Modeling post-  
916 depositional mixing of archaeological deposits. *Journal of Anthropological Archae-  
917 ology* 26 (4), 517–540.
- 918 Carrer, F., 2015. Interpreting Intra-site Spatial Patterns in Seasonal Contexts: an Eth-  
919 noarchaeological Case Study from the Western Alps. *Journal of Archaeological*  
920 *Method and Theory*, 1–25.
- 921 Cobo-Sánchez, L., Aramendi, J., Domínguez-Rodrigo, M., 2014. Orientation patterns  
922 of wildebeest bones on the lake Masek floodplain (Serengeti, Tanzania) and their  
923 relevance to interpret anisotropy in the Olduvai lacustrine floodplain. *Quaternary*  
924 *International* 322–323 (Supplement C), 277–284.
- 925 de la Torre, I., Benito-Calvo, A., 2013. Application of GIS methods to retrieve ori-  
926 entation patterns from imagery; a case study from Beds I and II, Olduvai Gorge  
927 (Tanzania). *Journal of Archaeological Science* 40 (5), 2446–2457.
- 928 Dibble, H. L., Chase, P. G., McPherron, S. P., Tuffreau, A., Oct. 1997. Testing the  
929 reality of a "living floor" with archaeological data. *American Antiquity* 62 (4), 629–  
930 651.
- 931 Diggle, P., 1985. A kernel method for smoothing point process data. *Applied Statistics*  
932 (*Journal of the Royal Statistical Society, Series C*) 34, 138–147.
- 933 Domínguez-Rodrigo, M., Bunn, H., Mabulla, A., Baquedano, E., Uribelarrea, D.,  
934 Pérez-González, A., Gidna, A., Yravedra, J., Diez-Martin, F., Egeland, C., Barba,  
935 R., Arraza, M., Organista, E., Ansón, M., 2014a. On meat eating and human evolu-  
936 tion: A taphonomic analysis of BK4b (Upper Bed II, Olduvai Gorge, Tanzania), and  
937 its bearing on hominin megafaunal consumption. *Quaternary International* 322–323,  
938 129–152.

- 939 Domínguez-Rodrigo, M., Bunn, H., Pickering, T., Mabulla, A., Musiba, C., Baquedano, E., Ashley, G., Diez-Martin, F., Santonja, M., Uribelarrea, D., Barba, R.,  
940 Yravedra, J., Barboni, D., Arriaza, C., Gidna, A., 2012. Autochthony and orientation  
941 patterns in Olduvai Bed I: a re-examination of the status of post-depositional biasing  
942 of archaeological assemblages from FLK North (FLKN). *Journal of Archaeological*  
943 *Science* 39 (7), 2116–2127.
- 945 Domínguez-Rodrigo, M., Cobo-Sánchez, L., Yravedra, J., Uribelarrea, D., Arriaza, C.,  
946 Organista, E., Baquedano, E., 2017. Fluvial spatial taphonomy: a new method for the  
947 study of post-depositional processes. *Archaeological and Anthropological Sciences*.
- 948 Domínguez-Rodrigo, M., Diez-Martín, F., Yravedra, J., Barba, R., Mabulla, A., Baquedano, E., Uribelarrea, D., Sánchez, P., Eren, M. I., 2014b. Study of the SHK Main  
949 Site faunal assemblage, Olduvai Gorge, Tanzania: Implications for Bed II taphonomy,  
950 paleoecology, and hominin utilization of megafauna. *Quaternary International*  
951 322–323, 153–166.
- 953 Domínguez-Rodrigo, M., García-Pérez, A., 07 2013. Testing the Accuracy of Different  
954 A-Axis Types for Measuring the Orientation of Bones in the Archaeological and  
955 Paleontological Record. *PLoS ONE* 8 (7), e68955.
- 956 Domínguez-Rodrigo, M., Uribelarrea, D., Santonja, M., Bunn, H., García-Pérez, A.,  
957 Pérez-González, A., Panera, J., Rubio-Jara, S., Mabulla, A., Baquedano, E., Yrave-  
958 dra, J., Diez-Martín, F., 2014c. Autochthonous anisotropy of archaeological ma-  
959 terials by the action of water: experimental and archaeological reassessment of the  
960 orientation patterns at the Olduvai sites . *Journal of Archaeological Science* 41 (Sup-  
961 plement C), 44–68.
- 962 Eberth, D. A., Rogers, R. R., Fiorillo, A. R., 2007. A practical approach to the study of  
963 bonebeds. In: Rogers, R. R., Eberth, D. A., Fiorillo, A. R. (Eds.), *Bonebeds. Genesis,*  
964 *Analysis, and Paleoecological Significance*. The University of Chicago Press, pp.  
965 265–332.
- 966 Enloe, J. G., 2006. Geological processes and site structure: assessing integrity at a Late  
967 Paleolithic open-air site in northern France. *Geoarchaeology* 21 (6), 523–540.
- 968 Eren, M. I., Durant, A., Neudorf, C., Haslam, M., Shipton, C., Bora, J., Korisettar,  
969 R., Petraglia, M., 2010. Experimental examination of animal trampling effects on  
970 artifact movement in dry and water saturated substrates: a test case from South India.  
971 *Journal of Archaeological Science* 37 (12), 3010–3021.
- 972 Fernández-López, S. R., 1991. Taphonomic concepts for a theoretical biochronology.  
973 *Revista Española de Paleontología* 6, 37–49.
- 974 Fiorillo, A. R., 1991. Taphonomy and depositional setting of Careless Creek Quarry  
975 (Judith River Formation), Wheatland County, Montana, U.S.A. *Palaeogeography,*  
976 *Palaeoclimatology, Palaeoecology* 81 (3), 281–311.
- 977 Frison, G. C., Todd, L. C., 1986. *The Colby Mammoth Site: Taphonomy and Archae-  
978 ology of a Clovis Kill in Northern Wyoming*. University of New Mexico Press.

- 979 García-Moreno, A., Smith, G. M., Kindler, L., Pop, E., Roebroeks, W., Gaudzinski-  
980 Windheuser, S., Klinkenberg, V., 2016. Evaluating the incidence of hydrological  
981 processes during site formation through orientation analysis. A case study of the  
982 middle Palaeolithic Lakeland site of Neumark-Nord 2 (Germany). Journal of Ar-  
983 chaeological Science: Reports 6, 82–93.
- 984 Giusti, D., Arzarello, M., 2016. The need for a taphonomic perspective in spatial analy-  
985 sis: Formation processes at the Early Pleistocene site of Pirro Nord (P13), Apricena,  
986 Italy. Journal of Archaeological Science: Reports 8, 235–249.
- 987 Harvati, K., Panagopoulou, E., Tourloukis, V., Thompson, N., Karkanas, P., Athanas-  
988 siou, A., Konidaris, G., Tsartsidou, G., Giusti, D., 2016. New Middle Pleistocene  
989 elephant butchering site from Greece. In: Paleoanthropology Society Meeting. At-  
990 lanta, Georgia, pp. A14–A15.
- 991 Hivernel, F., Hodder, I., 1984. Analysis of artifact distribution at Ngenym (Kenya):  
992 depositional and postdepositional effects. In: Hietala, H., Larson, P. (Eds.), Intrasite  
993 Spatial Analysis in Archaeology. Cambridge University Press, Ch. 7, pp. 97–115.
- 994 Hodder, I., Orton, C., 1976. Spatial Analysis in Archaeology. New Studies in Archae-  
995 ology. Cambridge University Press, Cambridge.
- 996 Hovers, E., Ekshtain, R., Greenbaum, N., Malinsky-Buller, A., Nir, N., Yeshurun, R.,  
997 2014. Islands in a stream? Reconstructing site formation processes in the late Middle  
998 Paleolithic site of 'Ein Qashish, northern Israel. Quaternary International 331, 216–  
999 233.
- 1000 Isaac, G. L., 1967. Towards the interpretation of occupation debris: Some experiments  
1001 and observations. Kroeber Anthropological Society Papers 37 (37), 31–57.
- 1002 Jammalamadaka, S., Sengupta, A., Sengupta, A., 2001. Topics in Circular Statistics.  
1003 Series on multivariate analysis. World Scientific.
- 1004 Karkanas, P., Tourloukis, V., Thompson, N., Giusti, D., Panagopoulou, E., Harvati, K.,  
1005 this issue. Sedimentology and micromorphology of the Lower Palaeolithic lakeshore  
1006 site Marathousa 1, Megalopolis basin, Greece. Quaternary International.
- 1007 Kluskens, S. L., 1990. Orientation and density analysis of stone artefacts at Combe-  
1008 Capelle Bas, Périgord, France. Master's thesis, University of Pennsylvania.
- 1009 Konidaris, G., Athanassiou, A., Tourloukis, V., Thompson, N., Giusti, D.,  
1010 Panagopoulou, E., Harvati, K., this issue. The skeleton of a straight-tusked elephant  
1011 (*Palaeoloxodon antiquus*) and other large mammals from the Middle Pleistocene  
1012 butchering locality Marathousa 1 (Megalopolis Basin, Greece): preliminary results.  
1013 Quaternary International.
- 1014 Krumbein, W. C., 1941. Measurement and geological significance of shape and round-  
1015 ness of sedimentary particles. Journal of Sedimentary Research 11 (2), 64–72.

- 1016 Kuiper, 1960. Tests concerning random points on a circle. Proceedings of the Koninklijke Nederlandse Akademie van Wetenschappen, Series A 63, 38—47.
- 1017
- 1018 Lenoble, A., Bertran, P., 2004. Fabric of Palaeolithic levels: methods and implications  
1019 for site formation processes. *Journal of Archaeological Science* 31 (4), 457–469.
- 1020 Lenoble, A., Bertran, P., Lacrampe, F., 2008. Solifluction-induced modifications  
1021 of archaeological levels: simulation based on experimental data from a modern  
1022 periglacial slope and application to French Palaeolithic sites. *Journal of Archaeo-*  
1023 *logical Science* 35 (1), 99–110.
- 1024 Lindsay, J. F., 1968. The development of clast fabric in mudflows. *Journal of Sedimen-*  
1025 *tary Research* 38 (4), 1242–1253.
- 1026 Macdonald, D. I. M., Jefferson, T. H., 1985. Orientation studies of waterlogged wood;  
1027 a paleocurrent indicator? *Journal of Sedimentary Research* 55 (2), 235–239.
- 1028 Malinsky-Buller, A., Hovers, E., Marder, O., 2011. Making time: ‘Living floors’,  
1029 ‘palimpsests’ and site formation processes – A perspective from the open-air Lower  
1030 Paleolithic site of Revadim Quarry, Israel. *Journal of Anthropological Archaeology*  
1031 30 (2), 89–101.
- 1032 Marwick, B., 2017. Computational reproducibility in archaeological research: Ba-  
1033 sic principles and a case study of their implementation. *Journal of Archaeological*  
1034 *Method and Theory* 24 (2), 424–450.
- 1035 Marwick, B., d’Alpoim Guedes, J., Barton, C. M., Bates, L. A., Baxter, M., Beavan,  
1036 A., Bollwerk, E. A., Bocinsky, R. K., Brughams, T., Carter, A. K., Conrad, C.,  
1037 Contreras, D. A., Costa, S., Crema, E. R., Daggett, A., Davies, B., Drake, B. L.,  
1038 Dye, T. S., France, P., Fullager, R., Giusti, D., Graham, S., Harris, M. D., Hawks, J.,  
1039 Heath, S., Huffer, D., Kansa, E. C., Kansa, S. W., Madsen, M. E., Melcher, J., Negre,  
1040 J., Neiman, F. D., Opitz, R., Orton, D. C., Przystupa, P., Raviele, M., Riel-Salvatore,  
1041 J., Riris, P., Romanowska, I., Smith, J., Strupler, N., Ullah, I. I., Vlack, H. G. V.,  
1042 VanValkenberg, N., Watrall, E. C., Webster, C., Wells, J., Winters, J., Wren, C. D.,  
1043 2017. Open science in archaeology. *SAA Archaeological Record* 17 (4), 8–14.
- 1044 McPherron, S. J., 2005. Artifact orientations and site formation processes from total  
1045 station proveniences. *Journal of Archaeological Science* 32 (7), 1003–1014.
- 1046 McPherron, S. J., Dibble, H. L., Goldberg, P., 2005. Z. *Geoarchaeology* 20 (3), 243–  
1047 262.
- 1048 Morton, A. G. T., 2004. Archaeological Site Formation: Understanding Lake Margin  
1049 Contexts. Vol. 1211 of International Series. British Archaeological Reports, Oxford.
- 1050 Nickel, B., Riegel, W., Schonherr, T., Velitzelos, E., 1996. Environments of coal forma-  
1051 tion in the Pleistocene lignite at Megalopolis, Peloponnese (Greece) - reconstruc-  
1052 tion from palynological and petrological investigations. *N. Jb. Geol. Palaont. A.* 200,  
1053 201–220.

- 1054 Ohser, J., 1983. On estimators for the reduced second moment measure of point pro-  
 1055 cesses. *Mathematische Operationsforschung und Statistik, series Statistics* 14, 63–  
 1056 71.
- 1057 Organista, E., Domínguez-Rodrigo, M., Yravedra, J., Uribe Larrea, D., Arriaza, M. C.,  
 1058 Ortega, M. C., Mabulla, A., Gidna, A., Baquedano, E., 2017. Biotic and abiotic pro-  
 1059 cesses affecting the formation of BK Level 4c (Bed II, Olduvai Gorge) and their bearing  
 1060 on hominin behavior at the site. *Palaeogeography, Palaeoclimatology, Palaeoec-  
 1061 ology* (in press).
- 1062 Orton, C., 1982. Stochastic process and archaeological mechanism in spatial analysis.  
 1063 *Journal of Archaeological Science* 9 (1), 1–23.
- 1064 Panagopoulou, E., Toureloukis, V., Thompson, N., Athanassiou, A., Tsartsidou, G.,  
 1065 Konidaris, G., Giusti, D., Karkanas, P., Harvati, K., 2015. Marathousa 1: a new Mid-  
 1066 dle Pleistocene archaeological site from Greece. *Antiquity Project Gallery* 89 (343).
- 1067 Petraglia, M. D., Nash, D. T., 1987. The impact of fluvial processes on experimen-  
 1068 tal sites. In: Nash, D. T., Petraglia, M. D. (Eds.), *Natural formation processes and*  
 1069 *the archaeological record*. Vol. 352 of *International Series. British Archaeological*  
 1070 *Reports*, Oxford, pp. 108–130.
- 1071 Petraglia, M. D., Potts, R., 1994. Water Flow and the Formation of Early Pleistocene  
 1072 Artifact Sites in Olduvai Gorge, Tanzania . *Journal of Anthropological Archaeology*  
 1073 13 (3), 228–254.
- 1074 Pewsey, A., Neuhauser, M., Ruxton, G. D., 2013. *Circular Statistics in R*. Oxford  
 1075 University Press.  
 1076 URL [http://www.ebook.de/de/product/21010817/arthur\\_pewsey\\_](http://www.ebook.de/de/product/21010817/arthur_pewsey_markus_neuhauser_graeme_d_ruxton_circular_statistics_in_r.html)  
 1077 [markus\\_neuhauser\\_graeme\\_d\\_ruxton\\_circular\\_statistics\\_in\\_r.html](http://www.ebook.de/de/product/21010817/arthur_pewsey_markus_neuhauser_graeme_d_ruxton_circular_statistics_in_r.html)
- 1078 Pierson, T. C., 2005. Distinguishing between debris flows and floods from field evi-  
 1079 dence in small watersheds. *USGS Numbered Series*, U.S. Geological Survey.
- 1080 R Core Team, 2017. *R: A Language and Environment for Statistical Computing*. R  
 1081 Foundation for Statistical Computing, Vienna, Austria.  
 1082 URL <https://www.R-project.org/>
- 1083 Ripley, B., 1977. Modelling spatial patterns. *Journal of the Royal Statistical Society,*  
 1084 *series B* 39, 172–212.
- 1085 Ripley, B., 1988. *Statistical inference for spatial processes*. Cambridge University  
 1086 Press.
- 1087 Ripley, B. D., 1976. The second-order analysis of stationary point processes. *Journal*  
 1088 *of Applied Probability* 13 (2), 255–266.
- 1089 Ripley, B. D., 1981. *Spatial Statistics*. John Wiley and Sons, New York.
- 1090 Schick, K. D., 1984. Processes of paleolithic site formation: an experimental study.  
 1091 Ph.D. thesis, University of California, Berkeley.

- 1092 Schick, K. D., 1986. Stone Age sites in the making: experiments in the formation  
1093 and transformation of archaeological occurrences. Vol. 319 of International Series.  
1094 British Archaeological Reports, Oxford.
- 1095 Schick, K. D., 1987. Modeling the formation of Early Stone Age artifact concentra-  
1096 tions. *Journal of Human Evolution* 16, 789–807.
- 1097 Schiffer, M. B., 1972. Archaeological Context and Systemic Context. *American Antiq-*  
1098 *uity* 37 (2), 156–165.
- 1099 Schiffer, M. B., 1983. Toward the identification of formation processes. *American An-*  
1100 *tiquity* 48 (4), 675–706.
- 1101 Schiffer, M. B., 1987. Formation processes of the archaeological record. University of  
1102 New Mexico Press, Albuquerque.
- 1103 Shackley, M. L., 1978. The behaviour of artefacts as sedimentary particles in a fluvialite  
1104 environment. *Archaeometry* 20 (1), 55–61.
- 1105 Sánchez-Romero, L., Benito-Calvo, A., Pérez-González, A., Santonja, M., 12 2016.  
1106 Assessment of Accumulation Processes at the Middle Pleistocene Site of Ambrona  
1107 (Soria, Spain). Density and Orientation Patterns in Spatial Datasets Derived from  
1108 Excavations Conducted from the 1960s to the Present. *PLOS ONE* 11 (12), 1–27.
- 1109 Texier, J.-P., 2000. A propos des processus de formation des sites préhistoriques / About  
1110 prehistoric site formation processes. *Paléo* 12 (1), 379–386.
- 1111 Toots, H., 1965. Orientation and distribution of fossils as environmental indicators. In:  
1112 Nineteenth Field Conference of the Wyoming Geological Association. pp. 219–292.
- 1113 Tourloukis, V., Thompson, N., Panagopoulou, E., Giusti, D., Konidaris, G., Karkanas,  
1114 P., Harvati, K., this issue. Lithic artifacts and bone tools from the Lower Palaeolithic  
1115 site of Marathousa 1, Megalopolis, Greece: preliminary results. *Quaternary Interna-*  
1116 *tional*.
- 1117 van Vugt, N., de Bruijn, H., van Kolfschoten, M., Langereis, C. G., 2000. Magneto-  
1118 and cyclostratigraphy and mammal-fauna's of the Pleistocene lacustrine Megalopo-  
1119 lis Basin, Peloponnesos, Greece. *Geologica Ultrajectina* 189, 69–92.
- 1120 Vaquero, M., Chacón, M. G., García-Antón, M. D., de Soler, B. G., Martínez, K.,  
1121 Cuartero, F., 2012. Time and space in the formation of lithic assemblages: The  
1122 example of Abric Romaní Level J. *Quaternary International* 247 (0), 162–181.
- 1123 Villa, P., 2004. Taphonomy and stratigraphy in european prehistory. *Before Farming*  
1124 2004 (1), 1–20.
- 1125 Voorhies, M., 1969. Taphonomy and population dynamics of an early Pliocene ver-  
1126 tebrate fauna, Knox County, Nebraska. *Contributions to Geology, University of*  
1127 *Wyoming Special Paper* 1, 1–69.

- 1128 Walter, M. J., Trauth, M. H., 2013. A MATLAB based orientation analysis of  
1129 Acheulean handaxe accumulations in Olorgesailie and Kariandusi, Kenya Rift. Journal  
1130 of Human Evolution 64 (6), 569–581.
- 1131 Watson, 1961. Goodness-of-fit tests on a circle. Biometrika 48 (1/2), 109–114.
- 1132 Wood, R. W., Johnson, D. L., 1978. A survey of disturbance processes in archaeological  
1133 site formation. In: Schiffer, M. B. (Ed.), Advances in archaeological method and  
1134 theory. Vol. 1. Academic Press, Ch. 9, pp. 315–381.
- 1135 Woodcock, N., Naylor, M., 1983. Randomness testing in three-dimensional orientation  
1136 data. Journal of Structural Geology 5 (5), 539–548.